Palaeogeography, Palaeoclimatology, Palaeoecology 694 (2026) 113744

Contents lists available at ScienceDirect

Palaeogeography, Palaeoclimatology, Palaeoecology

journal homepage: www.elsevier.com/locate/palaeo

Unveiling "Mid-Pliocene Warm Period" dynamics through multiproxy stratigraphic analysis: The Valdelsa Basin in Northern Apennines – Italy as a key archive

L. Milaneschi [a,*], G. Cornamusini [a,b], P. Conti [a,b], I. Martini [a], J. Maffei [a], F. Cifelli [c], M. Mattei [c], S. Da Prato [d], M.C. Alçiçek [e], L.M. Foresi [a,d]

[a] University of Siena, Department of Physics, Earth and Environmental Sciences, Siena, Italy
[b] University of Siena, Centre of Geotechnologies, San Giovanni Valdarno, Italy
[c] Roma TRE University, Department of Science, Rome, Italy
[d] CNR, Geosciences and Earth Resources, Pisa, Italy
[e] University of Pamukkale, Department of Geology, Denizli, Türkiye

ARTICLE INFO

Editor: M Elliot

Keywords:
Multiproxy stratigraphy
Mid-Pliocene Warm Period
Biostratigraphy
Paleomagnetism
Stratigraphy
Mediterranean

ABSTRACT

Neogene marine marginal basins are important archives for reconstructing Pliocene depositional, paleogeographical and paleoenvironmental evolution. This study focuses on a key succession from the Valdelsa Basin (Tuscany, Italy), which represents a significant example within the Southern Tuscan Neogene basin system, to provide new insights into the mid-Pliocene Warm Period (m-PWP ~3.3–2.9 Ma). To achieve this, a multiproxy integrated stratigraphic approach was applied to a succession of shallow marine, paralic, and continental deposits. The methodology combined physical stratigraphy, sedimentary facies analysis, micro- and macropaleontological content, planktonic foraminiferal biostratigraphy, paleomagnetism, and chemical investigations. The studied succession has been deposited during the Piacenzian, from the upper part of the MPL4b to the MPL5a of the Mediterranean planktonic foraminiferal zonal scheme, including the m-PWP. The integration of bio- and magnetostratigraphic data, allowed the identification of two magnetic inversions: C2An.2r to C2An.2n and C2An.2n to C2An.1r. The integration of litho- and biofacies correlations allows to outline the detailed stratigraphic architecture with significant paleoecological and paleoenvironmental insights, while the new bio- and magnetostratigraphic proxy data have refined the chronostratigraphic framework. Furthermore, comparing of the updated chronological framework with global $\delta^{18}O$ benthic stack allows a more precise identification of the main climatic events that led the Basin depositional evolution. The complex and articulated architecture of the shallow-marine to continental succession, along with the distribution of biofacies, show that depositional evolution in the basin occurred mainly under the control of eustatic fluctuations even though the basin was tectonically active. These fluctuations led to alternating transgressive and regressive phases that correlate clearly with major global climatic events, as evidenced by the $\delta^{18}O$ stack. This study thus identifies climatic forcing as the primary control on the Valdelsa Basin's Piacenzian depositional evolution.

1. Introduction

The mid-Pliocene Warm Period (m-PWP, between ~3.3 and ~2.9 Ma according to Lisiecki and Raymo, 2005) is the most recent period in Earth's history whose temperatures are similar to predicted for the near-future climate conditions in the context of global warming (Dowsett et al., 2012, 2021). The nature and variability of climate during the m-PWP is a potential indicator of how the Earth might respond to future warming. Furthermore, studying this period contributes to providing data to develop a series of integrated global-scale quantitative datasets that can be used in climate modelling experiments and for reconstructing environmental conditions (Dowsett et al., 2021). In this context, studying the evolution of sedimentary basins in relation to climate variation is crucial for understanding the link between global climate forcing and local-scale responses (e.g. eustatic fluctuations and associated ecological changes), in sensitive areas such as the

* Corresponding author.
E-mail address: lorenzo.milaneschi@unisi.it (L. Milaneschi).

https://doi.org/10.1016/j.palaeo.2026.113744
Received 26 November 2025; Received in revised form 17 February 2026; Accepted 20 March 2026
Available online 6 April 2026

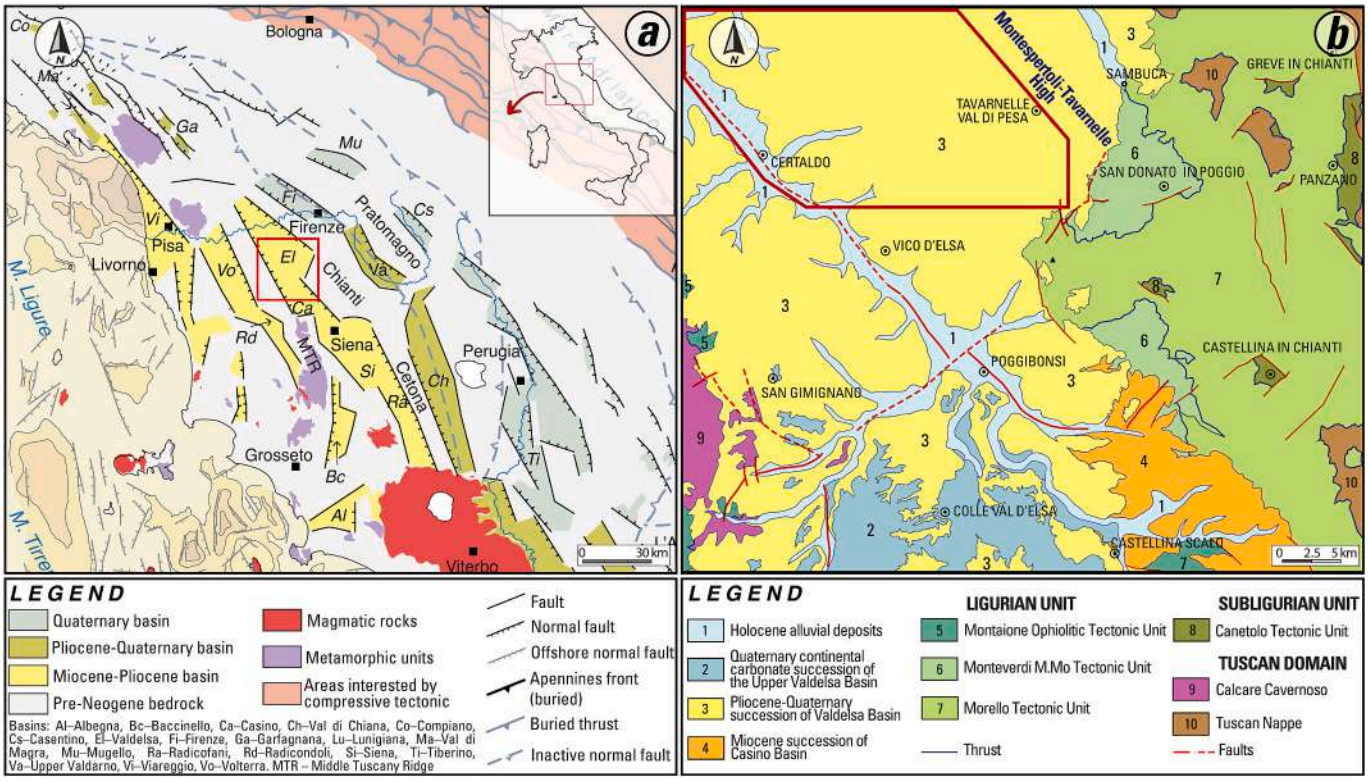

Fig. 1. Geological settings: *a*, Tectonic scheme of the Northern Apennines with main Neogene basins (Conti et al., 2022 modified). The red square indicates the area of Fig. 1b; *b*, tectonic scheme of the central-southern Valdelsa Basin (Cornamusini et al., 2025). The red polygon indicates the study area. (For interpretation of the references to colour in this figure legend, the reader is referred to the web version of this article.)

Mediterranean Basin. The Neogene basins of Tuscany, located in the Northern Apennines hinterland, represent key Mediterranean archives for understanding how climate changes and local tectonic processes influenced the development of sedimentary successions. These successions provide detailed records of the depositional and paleoenvironmental changes related to climatic fluctuations and/or tectonic processes (Capezzuoli et al., 2006; Riforgiato et al., 2011; Benvenuti et al., 2014; Nalin et al., 2016; Dominici et al., 2008; Aldinucci et al., 2019).

In this framework, a large part of the Piacenzian infill of these basins is of particular interest due to their development during the m-PWP, as exemplified by the Valdelsa Basin, one of the most significant Neogene basins in the hinterland of the northern Apennines.

The Valdelsa Basin preserves an expanded Piacenzian succession of shallow-marine, paralic, and continental deposits, offering a unique opportunity to link basin-scale dynamics with global climate forcing. This succession has been widely studied over the last few decades to investigate its complex and articulated stratigraphic architecture. New mapping for the Italian national geological cartography (CARG Sheet 286-Poggibonsi, Cornamusini et al., 2025) has yielded novel proxy data that facilitate high-resolution interpretation for such successions. Previous studies focused on physical stratigraphy, using both a lithostratigraphic approach (Dainelli and Videssot, 1930; Merla and Bortolotti, 1967; Merla et al., 1967; Bossio et al., 2002) and the identification of Unconformity Bounded Stratigraphic Units (Bromley and D' Alessandro, 1983; Benvenuti et al., 2014; Aldinucci et al., 2019). Regarding the age of these deposits, earlier studies focused on biostratigraphy, primarily using planktonic foraminifera and calcareous nannofossils (though biomarkers are often scarce, which makes dating challenging; cf. Giannelli et al., 1981; Bossio et al., 1993a, 2002; Capezzuoli et al., 2005) and magnetostratigraphy (Nalin et al., 2016).

Here, we present new integrated stratigraphic data from the central Valdelsa Basin, combining physical stratigraphy, sedimentary facies analysis, micropaleontology, planktonic foraminiferal biostratigraphy and paleomagnetism. This integrated approach allows us to: *i*) refine the chronostratigraphic calibration of the Upper Pliocene deposits in proximal marine and continental environments, where dating is usually challenging; *ii*) reconstruct the stratigraphic architecture model of the studied successions and the related paleoenvironmental dynamics, evaluating the role of climate; *iii*) characterise the paleoecological settings, the paleogeographical configuration, and the sedimentary response to paleoclimatic evolution during the Piacenzian climatic optimum.

2. Geological setting and stratigraphy

The Valdelsa Basin is one of the most representative and large basins in the hinterland of the Northern Apennines (Fig. 1). It is a long depression, NNW-SSE orientated, ~60 km long and ~25 km wide, delimited by the Chianti Mountains - Monte Albano Ridge to the east and by the Middle Tuscany Ridge (MTR) to the west. Its south-western sector is connected to the Siena Basin (Martini and Aldinucci, 2017; Martini et al., 2021), through a morpho-structural element known as Casino Basin. The Valdelsa Basin is also characterised in its central eastern sector by the presence of a buried NNW-SSE structural high called Montespertoli-Tavarnelle High (Fig. 1b), this structure delimits the Pesa sub-Basin to the east (Fig. 2b), which is bounded eastward by the Chianti Mountains (Benvenuti et al., 2014; Mirabella et al., 2022).

Contrasting hypotheses exist regarding the origin of the Valdelsa Basin, as well as similar basins of Tuscany, attributing it either to an extensional or a compressional tectonic setting. The first hypothesis attributes the genesis of the Valdelsa Basin to extensional-post-collisional tectonics that started in the Middle-Late? Miocene with a graben-half-graben or a bowl-shaped basin's geometry, which evolved into graben (Carmignani et al., 1995; Pascucci et al., 1999; Brogi, 2011; Martini et al., 2021; Mirabella et al., 2022). The second hypothesis

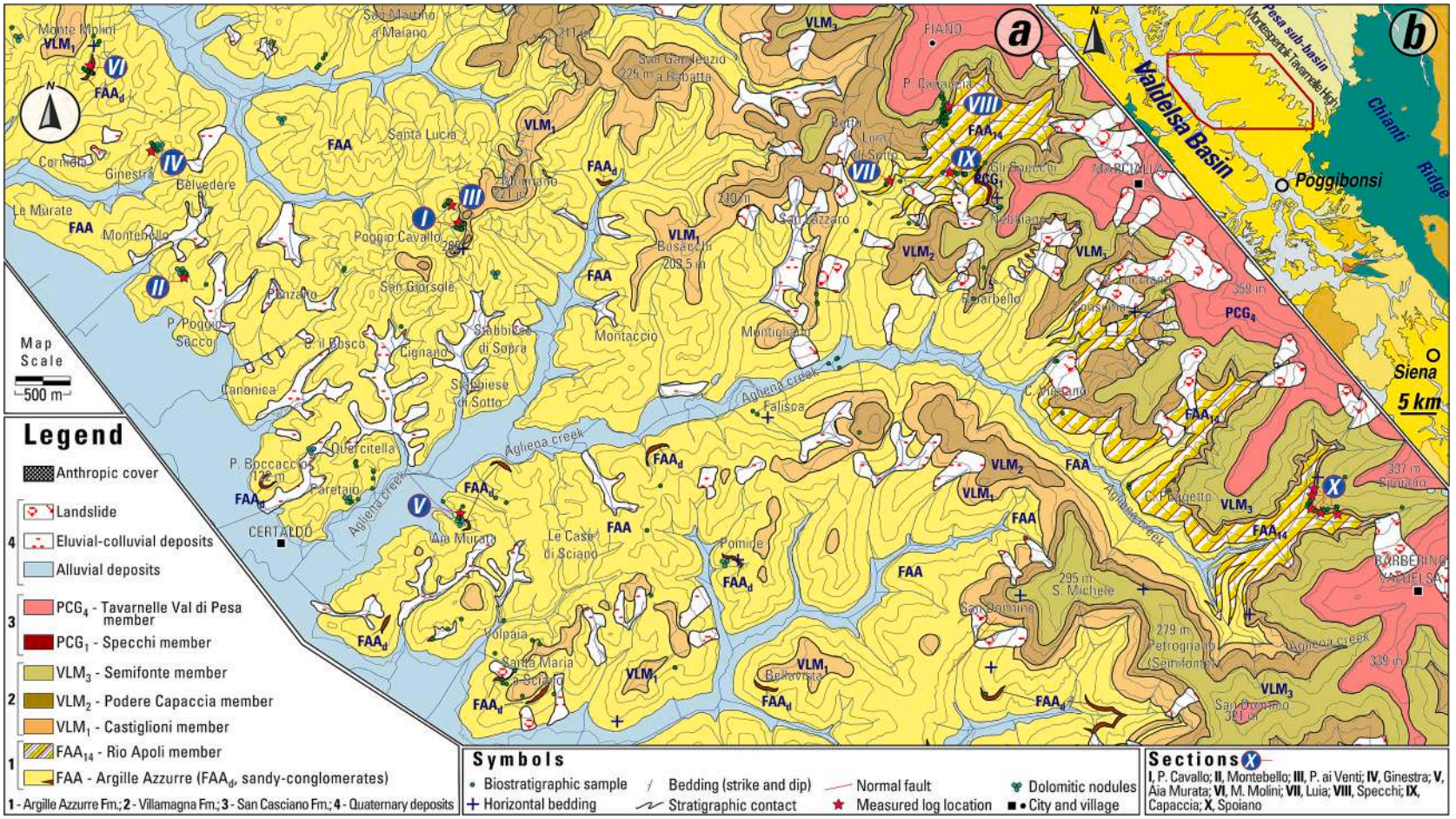

Fig. 2. *a*, Geological map of the study area. Lithostratigraphy from Cornamusini et al. (2025); *b*, tectonic sketch of central-southern sector of the Valdelsa Basin.

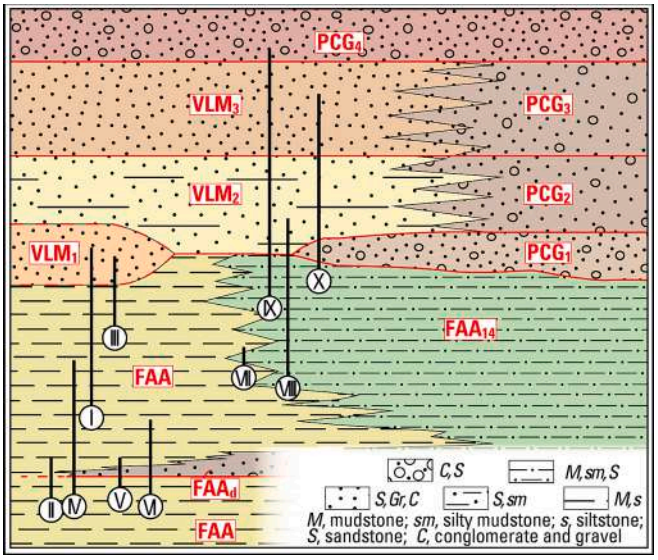

Fig. 3. Stratigraphic scheme of the central-eastern sector of the Valdelsa Basin. The black lines are the distribution of the measured and sampled sections of Fig. 2a. Lithostratigraphic units according to Cornamusini et al. (2025): FAA, Argille Azzurre (FAA14 - Rio Apoli member); VLM Villamagna formation (VLM1 - Castiglioni member, VLM2 - Podere Capaccia member, VLM3 - Semifonte member); PCG San Casciano formation (PCG1 - Specchi member, PCG2 - Cerbaia member, PCG3 - Montagnana member, PCG4 - Tavarnelle Val di Pesa member).

attributes the Basin's origin to compressive stress accumulated in the frontal zone of the Apennine chain. This stress led to the development of NE-vergent thrust and SW-vergent back-thrusts, forming thrust-top basins or complex interplays between major compressive tectonics and minor extensional tectonics affecting the hinterland basins (Boccaletti and Sani, 1998; Bonini and Sani, 2002; Sani et al., 2009; Benvenuti et al., 2014; Poneti et al., 2024).

In the Valdelsa Basin, Bossio et al. (1993a) documented two Pliocene-Pleistocene transgressive-regressive cycles separated by a regional unconformity. The first cycle was characterised by the Zanclean prevalent deposition of offshore mudstone (Bossio et al., 1993b, 2002). The second cycle, which is the focus of this study, occurred during the Piacenzian-early Gelasian, and was expressed by the deposition of marine and continental units, lithostratigraphically represented by the "Argille Azzurre" formation (FAA), "Villamagna" formation (VLM), "S. Casciano" formation (PCG) and their members (Figs. 2a and 3). During the deposition of this second cycle, from the earliest stages, a depocentral migration from east to west occurred, moving toward the MTR and depositing a great thickness of marine sediments (Capezzuoli et al., 2005). While marine facies transgressed onto the western margin, covering the pre-Neogene bedrock of the MTR as the basin deepened, a contemporaneous regression began in the eastern area with the deposition of mudstones to coarse-grained facies of infralittoral-coastal environments (Capezzuoli et al., 2005).

During the m-PWP, the central-eastern sector of the basin was characterised by the development of alluvial plains and lagoonal systems that transitioned southward into inner shelf environments. This paleogeographic configuration was subsequently modified by a Piacenzian regression affecting the eastern sectors, which triggered the diachronous deposition of coastal sandy facies of Villamagna formation (VLM) (Dominici et al., 1995; Bossio et al., 2002; Capezzuoli et al., 2005; Milaneschi et al., 2024; Cornamusini et al., 2025). While these coastal deposits graded laterally into coeval marine units, marine sedimentation persisted in the central-western areas, driven by the progressive basinward progradation of a deltaic system (Benvenuti et al., 2014; Aldinucci et al., 2019). This marine phase continued until the late Piacenzian, at which point it was truncated by the onset of lower Gelasian continental deposition of the S. Casciano formation (PCG). This transition was marked by the establishment of large-scale alluvial and deltaic systems, sourced from the adjacent mountain ranges, which prograded extensively into the basin (Canuti et al., 1966; Capezzuoli et al., 2005; Benvenuti et al., 2014). A synthetic lithostratigraphic correlation scheme is showed in Fig. 3.

3. Methods

3.1. Physical stratigraphy

Ten stratigraphic sections (locations are in Fig. 2), were selected and investigated. Lithology, sedimentary structures, geometries, texture, grain-size trends, and macrofossil content have been described for each section. Based on these parameters, different facies were categorised, grouping them into facies associations that represent different depositional environments.

3.2. Micropaleontology

Micropaleontological samples were collected through areal and linear methods. For each sample, 200 g of sediment were dried, weighed and reacted with a 10% aqueous solution of hydrogen peroxide (130 vol.). Once the reaction was complete, the sample was washed and sieved through a 63 μm mesh. The washing residue was dried under infrared lamps and weighed again. Micropaleontological analyses were carried out by observing the washed residues under a stereomicroscope identifying foraminifera and ostracods, through semi-quantitative analyses following the abundance classes proposed by Cita (1983). Biofacies were defined based on the faunal content of benthic and planktic foraminifera and ostracods. The genus and species of benthic and planktic foraminifera were determined using the following reference material: AGIP, 1982; Kennett and Srinivasan, 1983; Loeblich and Tappan, 1988; Iaccarino et al., 2007, www.foraminifera.eu, www.marinespecies.org and www.mikrotax.org (both pforams@mikrotax and bforams@mikrotax). The genus and species of ostracods were determined using the following reference material: Bonaduce et al. (1975), Athersuch et al. (1989), Medici et al. (2011) and Meisch (2000).

3.3. Paleomagnetism

3.3.1. Sampling and methods

127 oriented samples were collected from six stratigraphic sections using a battery-powered portable drill equipped with a water-cooled diamond bit. The cores were oriented in situ with a magnetic compass. The magnetic mineralogy of the sampled deposits was investigated using standard rock-magnetic techniques. Stepwise acquisition of isothermal remanent magnetization (IRM) was performed on 34 representative specimens using a pulse magnetizer up to a peak field of 2.7 T. A three-component IRM was also imparted to the same specimens using a 2G Enterprises model 660 pulse magnetizer at 2.7 T, 0.6 T, and 0.12 T along orthogonal axes. The samples were then thermally demagnetized following the method of Lowrie (1990).

The natural remanent magnetization (NRM) of one specimen per core was demagnetized through stepwise thermal demagnetization with small temperature increments (60–100 °C up to 180 °C, and 30–50 °C above 180 °C) until the NRM fells below the instrument sensitivity or random changes in paleomagnetic directions appeared. Some specimens

Table 1
Summary of the facies and their features. The code consists of a capital letter indicating the environment in which the facies occurs (C, continental; T, transitional; M, marine), a lowercase letter indicating the main lithology component (c, conglomerate and granules; s, sandstone; m, mudstone), and a progressive number.

Litho. Code	Facies description	Sedimentary structures	Depositional process
Cm1	Grey and greenish-grey mudstone and silty-mudstone with diffuse mottling. Occurrence of carbonate concretions, roots, carbonized vegetal remains and shells of continental gastropods	Plane-parallel lamination	Subaereal suspension deposition
Cm2	Dark grey to black mudstone in tabular bodies from 25 to 50 cm thick. Occurrence of carbonized vegetal remains, whitish millimetric to centimetric carbonate concretions and thin shells of continental gastropods (*Melanopsis* and *Theodoxus*)	Slickendside and shrink-swell features	Organic matter accumulation in waterlogged conditions due to the presence of a high water-table
Cm3	Brownish to reddish mudstone in tabular bodies from 20 to 45 cm thick. Occurrence of models of roots life-position, continental mollusk shell fragments and iron-manganese concretions up to 10 cm	Structureless	Pedogenesis processes in oxidizing and subaerial settings
Cm4	Light blue to dark blue mudstone with fragments of decalcified shells of mollusks, especially thin-shelled continental gastropods	Bioturbation and locally weakly lamination	Deposition in low-energy settings in fresh water
Cm5	Silty mudstone and siltstone in thin tabular layer 1–2 cm thick	Plane-parallel lamination	Unconfined sheet flows
Cs1	Lenticular bodies of brownish medium to coarse sandstone and silty sandstone. Commonly embedded in mudstone of Cm1 lithofacies. Occurrence of erosional basal pebbly lag	Trough-cross stratification	Dune migration in ribbon-like channels embedded in alluvial plain mudstones
Cc1	Heterometric clasts in tabular and lenticular bodies of 5 up to 10 cm thick from pebble to small cobble within sandy matrix. Vegetal remains are locally present	Locally clasts embrication	Unidirectional flow transport
Cc2	Lenticular or plane-concave bodies locally amalgamated, up to 50 cm thick, consisting of heterometric sub-rounded pebbles and cobbles with lenses composed of granules and sands or mud. Occurrence of carbonized vegetal rests and scattered carbonate concretions	Marked erosional base, internal cross-stratification and clast embrication	Confined flow in channels with high energy event.
Cc3	Heterometric clasts to matrix supported conglomerate composed of small to very large cobbles in coarse sandy matrix in crudely sub-horizontal tabular bodies. Occurrence of rare carbonized vegetal rests and mud clasts	Locally clasts embrication, internal erosional surfaces	Stream-flood
Tm1	Greyish mudstone and silty mudstone with carbonized vegetal rests and decalcified shell fragments. Occurrence of brackish water faunas	Bioturbation or thinly lamination	Deposition in low-energy settings in brackish water
Ts1	Medium to coarse sandstone with centimetric thick small to medium pebble intercalations. Occurrence of clay chips and centimetric mud clasts composed of mudstone containing brackish or freshwater faunas	Occurrence of clinoform and locally erosional basal pebbly lag	Prograding unconfined flows. High-energy events produce basal scouring and cannibalization of lagoonal and/or continental close deposits
Ts2	Alternance of coarse to very coarse well sorted sand, granules and heterometric conglomerate (from 1 to 6–8 cm thick), in beds of 20–40 cm thick. The sand portions are usually affected by widespread oxidation. Rare intercalations of silty sand containing shell fragments. Occurrence of dispersed mud clasts, carbonized vegetal rests and rounded shells of *Ostrea*	Locally occurrence of open-work texture in conglomerate; trough-cross bedding and lamination in sandy portion of lithofacies. Coarsening upward trends	Unconfined flows with sediment affected by winnowing processes due to waves in shallow-marine settings
Mm1	Greyish-blue mudstone and silty mudstone. Occurrence of abundant fossils in life position, scattered or concentrated in levels and of rare sulphide spherules and very rare glauconite grains. Locally presence of shell-beds	Bioturbation and rare fine plane-parallel lamination	Suspension deposition in marine setting
Ms1	Fine to very fine light blue sandstone. Occurrence of large carbonized wood and vegetal remains, gastropods models and centimetric carbonatic nodules	Bioturbation e and finely plane-parallel lamination. Very rare hummocky-cross stratification and fluid-escape structures	Suspension deposition with minor traction
Ms2	Yellowish medium sorted sandstone, locally cemented with thin pebble intercalations. Occurrence of macrofossils, carbonized vegetal rests and oxides	Plane-parallel lamination and trough-cross stratification. Occurrence of bioturbation	Deposition under wave action. Locally occurence of three-dimensional dunes in shallow-marine environment
Lag	Small and medium pebbles to medium well-rounded cobbles, composed of limestone and subordinate radiolarite, locally characterised by the presence of coarse to very coarse sandy matrix rich in shelly detritus. Pervasive clasts bioerosion and encrustations	Clasts embrication, isoorientation of bioclasts, locally open-work texture and coarsening upward trend	Transgressive lag in shoreface marine setting characterised by winnowing processes

Table 2
Summary of the facies association and their features.

Facies Ass.	Lithofacies	Main features	Macrofossils	Sedimentary environment	Formation/ Member
F1	Cm1, Cs1, Cm2, Cm3	Mudstones of Cm1 with interbedded lenticular bodies of Cs1 and subordinated tabular dark and red horizon of Cm2 and Cm3	*Theodoxus* and *Melanopsis*. In Cm2 terrestrial mollusks, rodents (*Moscardinus*?), fresh-water fish teeth, lizard jaws, bat molars occur	Alluvial plain with presence of ribbon-like channel. Organic matter accumulation and pedogenesis processes may occured	FAA3, VLM3
F2	Cc3, Cc2, Cm1	Amalgamation of Cc3 bodies with intercalation of Cm1	No fossils	Gravel-sand bed fluvial channel locally topped by alluvial plain deposits	PCG1
F3	Cm4, Cm5	Bodies mainly composed of Cm4 with subordinated thin layer of Cm6	Terrestrial shell fragments	Lacustrine / Fresh-water pond punctuated by sediment input by river flooding	FAA3, VLM3
F4	Ms2, Lag	Decimetric to metric bodies of Ms2 with intercalation of Lag	*Ostrea edulis* with subordinated *Crassostrea gryphoides, Panopea glycymeris, Glycymeris insubrica* and barnacle fragments	Upper shoreface - Foreshore	FAA, VLM1, VLM2, VLM3
F5	Ms1, Mm1, Lag	Metric bodies of Ms1 with millimetric to centimetric levels of Mm1. Rare intercalations of bioeroded and encrusted pebbly-cobbly horizon also occurred	*Ostrea edulis, Pelecyora brocchii, Venus* spp., *Glycymeris insubrica, G. pilosa, G. insubrica, Tellina* sp., *Bolinus brandaris*, *Ocenebra erinaceus, Natica tigrina, Heliacus* sp., *Helmintiha vermicularis, Murex* sp., *Dentalium fossile* and barnacle fragments. Occurrence in Lag of *Lithophaga, Rocellaria* and sponge borings (*Gastroaechnolithes* and *Entobia* ichnogenera) large barnacles, *Ostrea* and serpulids encrustation	Lower shoreface - Prodelta	FAA, VLM2
F6	Mm1, Ms1	Metric bodies of Mm1 with centimetric intercalations of Ms1. Carbonatic nodules is exclusively of this facies association	*Amussium cristatum, Chlamys multistriata, C. varia, Anadara gibbosa, Mytilus* sp., *Aphorrais uttingeriana, A. pespelecani, Xenophora infundibulum, Capulus* sp., *Conus brocchii, Conus* sp., *Natica tigrina, Naticarius* sp., *Solatia hirta, Hadriania* sp., *Euthria cornea, Cymathium dodorleni, Bathytoma cataphracta, Petalochoncus intorsus* and *Thylacoides arenarius*, *Dentalium fossile*, *D. sexangulum, Ditrupa* sp., *Dendrophyllia cornigera*, echinoids and bryozoans	Offshore - Inner shelf	FAA
F7	Tm1	Monotonous decimetres-thick of Cm5 rich in carbonized vegetal rests	Mainly decalcified gastropods and subordinately *Cerastoderma* and *Cerithium*	Hypoialine lagoon	FAA3, VLM2, VLM3
F8	Ts1, Cc1	Decimetric to metric bodies of Ts1 with Cc1 intercalations	*Ostrea* fragments	Deltaic deposition punctuated by higher energy episodes eroding unconsolidated lagoonal and/or continental deposits	VLM2, VLM3
F9	Ts2, Cc1	Bodies of Ts2 with common intercalations of Cc1	*Ostrea* and barnacles fragments	Mouth bar	FAAd
F10	Cc2, Cs1	Decimetric to metric crude stratified tabular bodies of Cc2 with subordinated Cs1	No fossils	Fluvio-alluvial	PCG4

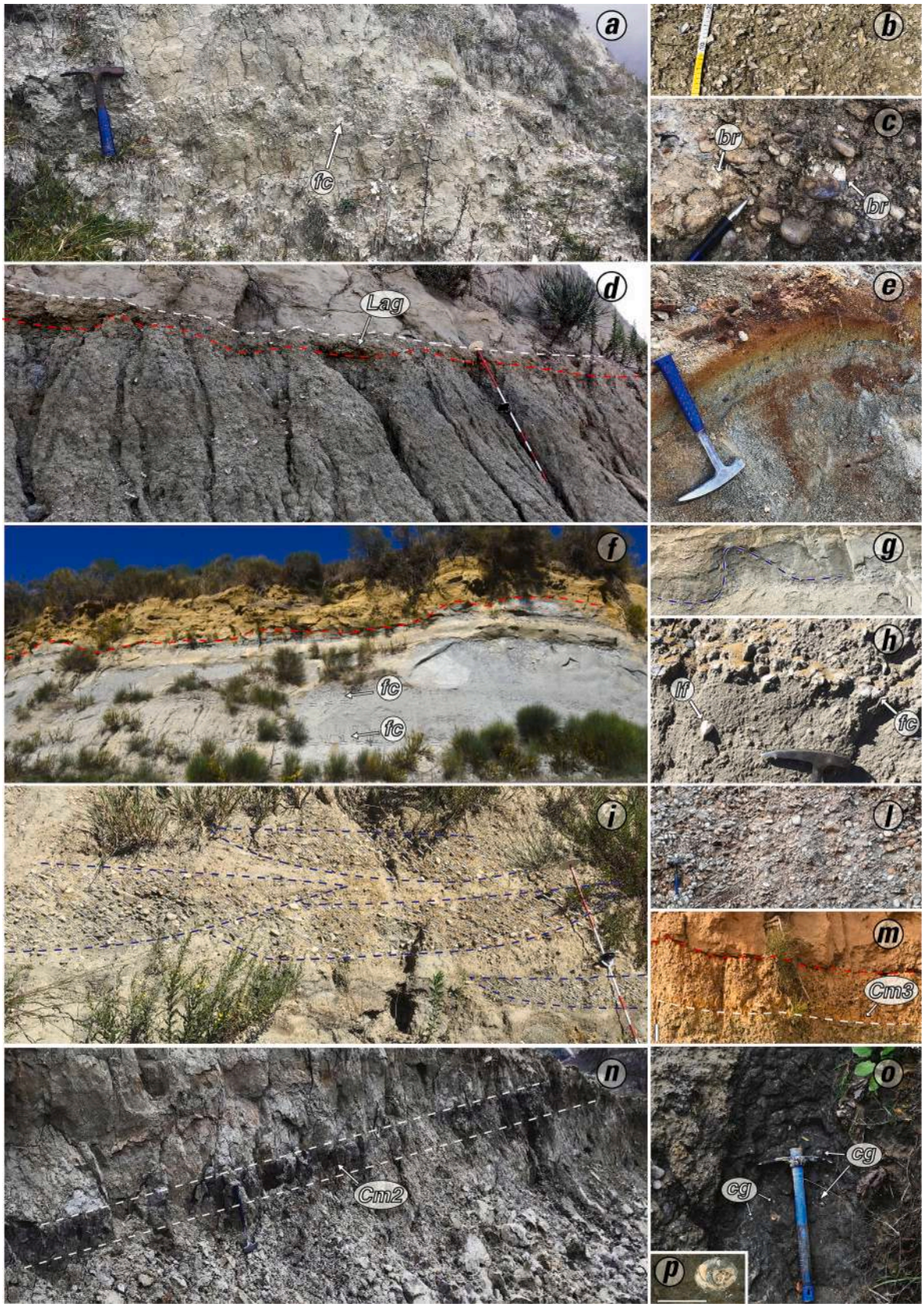

(caption on next page)

Fig. 4. Main representative facies and facies association. *a*, grey-bluish mudstone with fossils concentration (*fc*) of serpulids and bivalves (Mm1 facies at P. ai Venti section); *b*, *Ostrea* fragments concentration in Mm1 bluish mudstone at M. Molini section; *c*, heterometric subangular to subrounded conglomerate, with barnacle's encrustation (*br*), in very coarse sand matrix of Ts2 facies; *d*, erosive contact between grey mudstone of Cm1 and Lag (red dashed line) and with this last and bluish very fine sandstone of Ms1 at Spoiano section (white dashed line); *e*, very coarse well-sorted sandstone with thin bed of small carbonatic pebbles and pervasive oxidation; *f*, erosive contact between F5 and F8 facies association at Spoiano (fc, indicates the fossil concentrations); *g*, large scale soft-deformation structure in marine fine sandstone of F5 (white bar is 10 cm); *h*, fossils-rich horizons (*fc*) of marine mollusks, with bivalves in life position (*lf*) in fine grey sandstone; *i*, cross-stratification in clast-supported conglomerates of F10 facies association; *l*, channelized conglomeratic bodies with plane-concave geometry, composed of conglomerates which show an internal inclined stratification (F2), in floodplain mudstone (F1); *m*, erosive contact (red line) between grey-greenish mudstone (F1) with pedogenized horizon (Cm3) and coarse grained sandstone with scattered pebbles close to Specchi section (white bar is 10 cm); *n*, tabular dark organic-rich muddy horizon (Cm2) interbedded in Cm1 mudstone at Specchi section; *o*, detail of the black mudstone of Cm2 facies characterised by the presence of continental gastropods (*cg*); *p*, detail of a continental gastropod in Cm2 (white bar is 1 cm). (For interpretation of the references to colour in this figure legend, the reader is referred to the web version of this article.)

were also subjected to alternating-field (AF) demagnetization to compare their behavior with thermally demagnetized samples. AF demagnetization was carried out in 5 mT increments up to 50 mT, and 10 mT increments up to 80 mT.

All specimens were measured with a 2G Enterprises DC-SQUID (superconducting quantum interference device) cryogenic magnetometer located in a shielded room at the INGV Paleomagnetism Laboratory (Rome, Italy). Data analysis was performed using *Remasoft 3.0* software (Chadima and Hrouda, 2006). Characteristic remanent magnetization (ChRM) directions were determined by principal component analysis (PCA; Kirschvink, 1980). Virtual geomagnetic poles (VGPs) for each sample were calculated from the ChRM vectors.

4. Results

4.1. Litho- and biofacies: interpretation, paleoenvironmental and paleoecological meaning

Lithofacies are described in Table 1 and organized in ten facies associations (Table 2). They can be grouped in three main environmental groups: *i*) continental; *ii*) transitional; *iii*) shallow-water marine (Table 2). The main lithological features of these facies associations, their paleodepositional environment, biofacies, macrofossils content and paleoecological significance are described below. The complete list of main features and fossiliferous content is provided in Table 2, which also includes the 1:50′000 scale formational codes (Fig. 2), within which the facies associations have been identified.

4.1.1. Continental deposits

Continental deposits are well-exposed in the eastern sector of the study area. They are mainly represented by muddy alluvial sediments (F1 facies association, Table 2). The alluvial plain mudstones are characterised by the presence of tabular organic-rich horizons, dark grey to black in colour (Cm2 facies, Table 1; Fig. 4n, o), in which rodents and other vertebrate rests occurred (complete description in Table 2). These horizons originated under waterlogged, poorly drained, and reducing conditions, are typically associated with relative base-level rise phases driven by the creation of accommodation space (Wright and Marriott, 1993; Retallack, 2001; Holz et al., 2002; Mack et al., 2010; Jerrett et al., 2011; Benvenuti et al., 2021). Paleosols (Cm3 facies) are also present in F1 (Fig. 4m), and they are characterised by calcic features and the presence of common roots in life position, suggesting a genesis in well-drained, arid and semi-arid conditions, according to the IUSS (IUSS Working Group WRB, 2015). Coarse-grained sandy lenticular bodies (Cs1 facies), commonly occur within muddy alluvial deposits and can be interpreted as isolated, ribbon-like channels that evolve upwards into multi-storey channels in the succession, suggesting a progressive decrease in the accommodation rate (Aldinucci et al., 2019). The F1 facies association is abruptly eroded by F2 fluvial conglomerates indicating a decrease in accommodation space and consequent incision of the underlying continental floodplain mudstones (Fig. 5). In Spoiano section, F2 is topped by F1 mudstone (Fig. 4d), which is in turn truncated by an erosive surface, similarly to what has been observed and described by Aldinucci et al. (2019) in the Specchi and Capaccia sections area. The lacustrine F3 facies association is not recurrent and has been recognized in the Specchi and Spoiano area (Fig. 4). Here the monotonous Cm4 structureless or subordinated thinly laminated bluish mudstones is typically characterised by the presence of ostracods of the B8 biofacies, including *Candona* cf. *candida*, *Darwinula stevensoni* and *Potamocypris* cf. *zschokkei*. Finally, the F10 facies association, occurring in Capaccia section (Fig. 4) and common documented in the eastern sector of the study area, is characterised by the decimetric to metric crude stratified tabular bodies marked by erosional bases which attest the onset of fluvio-alluvial settings at the top of the succession (Fig. 5l).

4.1.2. Transitional deposits

These deposits are represented by three facies associations (F7, F8 and F9), which indicate transitional environments (Table 2). These associations have mainly been recognised in the eastern section of the study area (Figs. 2 and 4). The lagoonal facies (F7) was identified only in the easternmost sector and consists exclusively of monotonous structureless or locally thinly laminated greyish mudstone and silty mudstone rich in carbonized vegetal remains and decalcified mollusk shells. The macrofossils content includes mollusks as *Cerithium* sp. and *Cerastoderma* sp., while the micropaleontological assemblage is composed mainly of *Ammonia tepida* (Plate 1, figs. 12a-b), rare *Aubignyna perlucida* and *Miliammina fusca* among foraminifera, and of *Cyprideis torosa*, *Loxoconcha ovulata*, *Xestoleberis plana* and rare allochthonous valves of *Cypria ophtalmicica* among the ostracods. The physical and faunal content of this facies is indicative of a hypoialine lagoon (B2 biofacies, see Table 3). The F8 and F9 facies associations refer to a deltaic depositional setting of delta front and gravelly-sandy mouth bar, respectively (Table 2). The F9 facies association mostly outcrops in the central sector of the study area, where it is interbedded through an erosional base in the greyish-blue mudstone of F6 or very fine sandstone of F5. Locally, the onset of F9 is preceded by a shallowing-upward trend, as evidenced by the replacement of F6 by F5, coupled with a decrease in bathymetry as indicated by the rapid transition from a relatively deep-water to a shallow-water foraminiferal assemblage (e.g. log VI of Fig. 5). This is followed by an abrupt disappearance of marine micro- and macrofauna at the onset of transitional and continental facies association (F9 and F1), which suggests a relative fall in base-level (Catuneanu, 2022; Holland, 2023). The F8 facies association, mainly composed of sandstone, characterised by the presence of clinoforms, and subordinated pebbly and cobbly intercalations rests on a marked erosive surface on very fine bluish marine sandstone of F5 (Fig. 4f). This facies association, referred to a delta front facies, where present, can be found in alternation with marine muddy or sandy facies association (F5 and F4 in section IX) suggesting high frequency fluctuations in response to sea level or clastic supply. The pebbly-cobbly levels of the delta front facies association (F8) contain mud clasts (up to 10 cm) characterised by brackish and freshwater micropaleontological assemblages (B2 and B8 biofacies).

4.1.3. Shallow-water marine deposits

These deposits sedimented along a deepening gradient, from the upper shoreface (F4), to the lower shoreface to prodelta (F5), to the

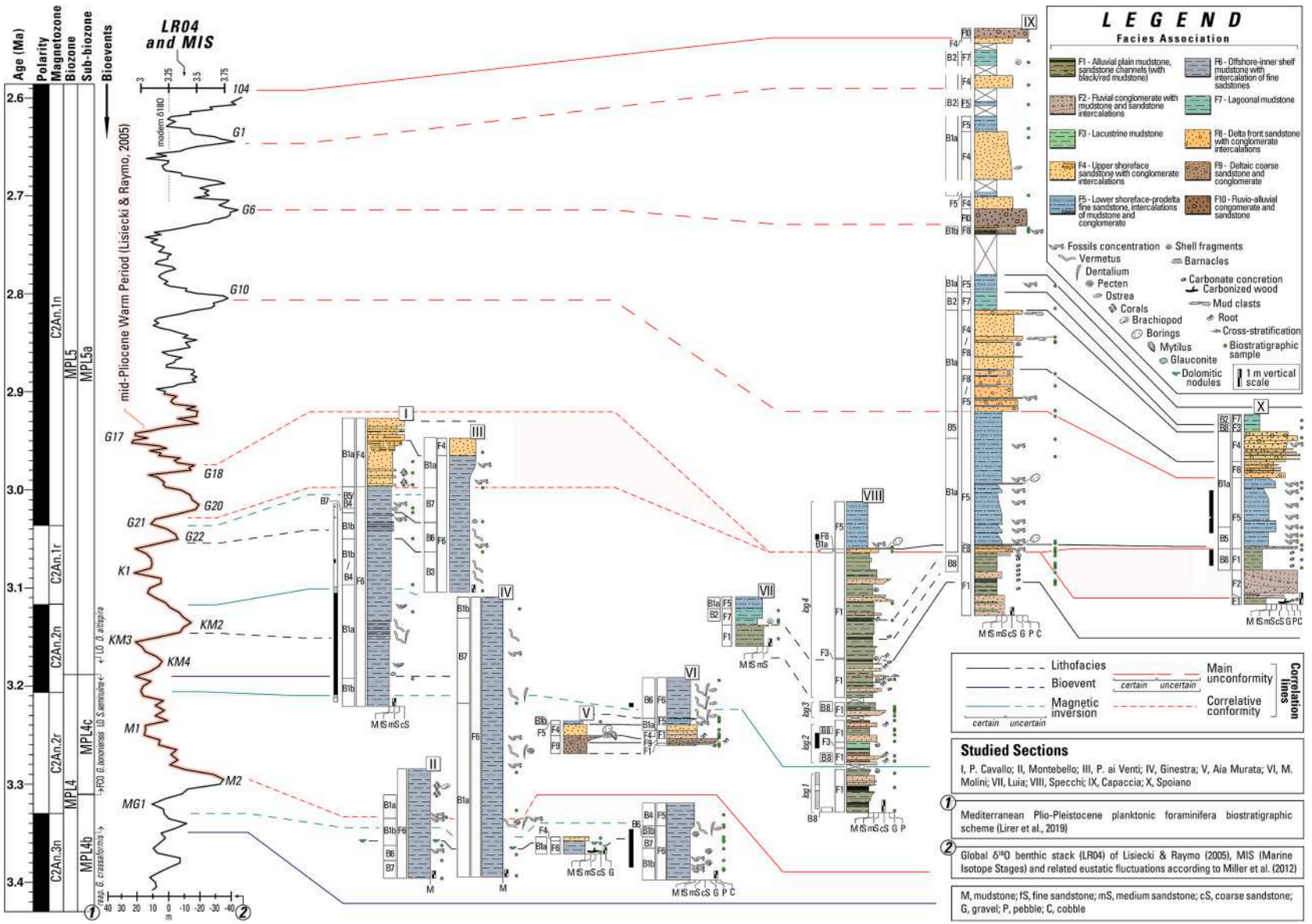

Fig. 5. *a*, Correlation framework of the studied sections. Biostratigraphy from Lirer et al. (2019). The global benthic $\delta^{18}O$ stack of Lisiecki and Raymo (2005), scaled to the global eustatic sea level according to Miller et al. (2012). See Table 2 for facies association (F*) and Table 3 for biofacies (B*).

(caption on next page)

Plate 1. 1*a-b*, *Globigerinoides elongatus* (M. Molini - LM202); 2, *Globoturborotalita apertura* (Ginestra - LM271); 3*a-b-c*, 4*a-b-c*, *Globorotalia crassaformis* (areal sample - LM222; M. Molini - LM196); 5*a-b-c*, *Globorotalia bononiensis* (Montebello - LM142); 6*a-b*, *Neogloboquadrina acostaensis* (M. Molini - LM215); 7, 8, *Sphaeroidinellopsis seminulina* (P. Cavallo - LM147; Ginestra - LM273); 9, *G. ruber* (Montebello - LM142); 10*a-b*, *G. quadrilobatus* (P. Cavallo - LM240); 11, 12*a-b*, *Ammonia tepida* (Capaccia - LM46; Luia - LM67); 13, *Nonion boueanum* (Capaccia - LM45); 14*a-b*, *Pullenia bulloides* (areal sample - LM200); 15*a-b*, *Cancris auriculus* (P. Cavallo - LM240); 16*a-b*, *Lobatula lobatula* (Capaccia - LM48); 17*a-b*, *Oridorsalis umbonatus* (M. Molini - LM196); 18, *Elphidium crispum* (areal sample - LM266); 19*a-b*, *A. beccarii* (areal sample - LM164); 20, *Planorbulina mediterraniensis* (P. Cavallo - LM137); 21, *Pyrgo bulloides* (P. Cavallo - LM140); 22, *Uvigerina peregrina* (P. Cavallo - LM138); 23, *Quinqueloculina seminulum* (Spoiano - LM81); 24, *Reussella spinulosa* (areal sample - LM82); 25, 26, fish teeth (areal samples - LM170, LM255); 27; Holothuridea sclerite (M. Molini - LM213); 28, *Rectuvigerina siphogenerinoides* (areal sample - LM178); 29, *Martinottiella communis* (M. Molini - LM196). White bar is 100 μm.

offshore (F6). The F4 represents an upper shoreface environment, characterised by the presence of wave action and punctuated by continental input. The macrofossil content is mainly characterised by common *Ostrea edulis,* and subordinate *Crassostrea gryphoides*. F4 is totally characterised by the occurrence of B1a sub-biofacies defined by abundant *Ammonia beccarii, Elphidium crispum* and *Nonion boueanum* (Plate 1, figs. 13, 18, 19a-b), suggesting a deposition in the inner part of the infralittoral zone (Table 2 and 3). Facies association F5 has a higher macrofossil content than F4, with common occurrence of *O. edulis*, Veneridae (e.g. *Venus multilamella, Pelecyora brocchii* (Plate 2, fig. 22) and gastropods such as *Aphorrais* spp., *Conus* sp., *Bolinus brandaris*, and *Helminthia vermicularis* (Table 2; Plate 2, figs. 2, 7, 15, 17). Bivalves are usually preserved in life position or concentrated in beds of disarticulated valves (Fig. 4f, h), ranging from densely to loosely packed (sensu Kidwell and Holland, 1991), representing autochthonous to parautochthonous accumulation formed during storm events, as also documented by the presence of locally hummocky-cross stratification structures. The recognition of Lag facies at the base of F5 facies association, indicates phases of relative sea-level rise, characterised by low clastic input and sedimentary stasis, as evidenced by the proliferation of bioeroders and encrusted organisms and very rare presence of glauconite grains. The deposits of this facies in the study area lie directly on the alluvial plain mudstone F1 or fluvio- and deltaic F2 and F8 facies association, (Fig. 4d). Furthermore, the occurrence in F5 of large *Glycymeris pilosa* (Plate 2, fig. 21), up to 15 cm in diameter, and the overall macrofauna and microfauna assemblage suggests the presence of vegetated substrates and a paleodepth of approximately 10 m (Peharda et al., 2019). Finally, F6 is characterised by thick metric to decimetric bodies of monotonous and mainly bioturbated bluish-grey mudstone referred to the offshore environment. In the central Basin area, gregarious organisms such as vermetiids and scaphopods are common with abundant concentration of *Petalochoncus intorsus*, *Thylacoides arenarius, Dentalium* spp. (Plate 2, figs. 1, 5).

The F6 is characterised by the presence of a laterally discontinued horizon of heterometric greyish carbonate nodules (Montebello, Aia Murata, Ginestra and Poggio Cavallo sections, Fig. 2). X-ray diffraction (XRD) and X-ray fluorescence (XRF) analyses, performed using Philips PW1830 diffractometer and portable Vanta Olympus M-Series analyser, show that these nodules consist primarily of dolomite and subordinate quartz, iron-rich clinochlore and muscovite (Fig. 8d).The B6 and B7 biofacies (Table 3), distinguished by their characteristic species, have been recognized only in this last facies association. Both biofacies are characterised by distinctive species of *Globigerinoides* (*G. elongatus, G. quadrilobatus, G. ruber, G. trilobus*) and *Globigerina* (*G. bulloides* and *G. falconiensis*), Plate 1, figs. 1a-b, 9. In particular, B7 is enriched in other species such as *Globoturborotalita apertura* (Plate 1 fig. 2), *G. decoraperta*, *Globigerinella aequilateralis*, *G. calida praecalida*, *Neogloboquadrina acostaensis* and *N. planispira* and rare *Turborotalita quinqueloba*, (Plate 1, fig. 6a-b). These two biofacies provide evidence of the deepest bathymetric conditions reached in the Basin during the Piacenzian. Furthermore, within the shallow-marine facies deposits, biofacies B3, B4 and B5 are less common but paleoecologically significant. In fact, biofacies B3 and B4, characterised by common or abundant dysoxic and suboxic taxa, are typical of the bluish, thinly laminated mudstone of F6, indicating a seafloor with underoxygenated conditions. Biofacies B5, characterised by the presence of common and diversified Miliolids with sandy substrate affinities (as *Quinqueloculina* spp., Plate 1, fig. 23 and *Triloculina oblonga*), and the absence of echinoids, suggest slightly higher salinity conditions (Murray, 1968, 2006). In general, the macro- and microfossils content of F6 suggests a deposition within a range from the infralittoral to the inner part of the circalittoral zone. Regarding biomarkers, planktonic foraminifera are generally rare in the shallow-water marine deposits. The stratigraphically lowermost samples, collected in the Argille Azzurre (FAA) from the depocentral Basin area, contain well-preserved specimens of *Globorotalia crassaformis* and *G. bononiensis*, Plate 1, figs. 4a-b-c, 5a-b-c. *Sphaeroidinellopsis seminulina* mostly characterised by the absence of the typical cortex (Plate 1, figs. 7, 8). In addition, among benthic foraminifera, *Textularia jugosa* has been identified in the lowest samples of the Argille Azzurre (Montebello area, Fig. 2). According to Capezzuoli et al. (2005), this benthic species in Tuscany occurs exclusively in the Piacenzian.

4.2. Paleomagnetic data

4.2.1. Natural remanent magnetization (NRM)

Samples for magnetostratigraphic analysis were collected from the Poggio Cavallo, Monte Molini, Specchi composite, and Spoiano sections (Fig. 5).

A total of 41 core samples were collected from the P. Cavallo section (site VE02), and a ChRM component was successfully isolated in 35 of them. At 1.25 m from the base, a ChRM component oriented upward and to the south was isolated between 120 °C and 360 °C indicating a reverse polarity. From 1.25 m to 15–16 m, the samples display ChRM components isolated between 20 and 30 mT and 50–60 mT (AF demagnetization), or between 20 and 120 °C and 360–400 °C (thermal demagnetization), oriented downward and to the north (Fig. 6d). Samples from approximately 16 m to the top show a low-temperature component (up to 180 °C) pointing down and northward, interpreted as a viscous remanent magnetization, followed by a well-defined reverse ChRM component oriented south and upward, isolated up to 360–440 °C (Fig. 6c). This indicates a reverse polarity interval.

In the M. Molini section (site VE01), 30 samples were collected from two stratigraphic intervals (~2 to ~7 m and ~15–16 m from the base). Most samples were thermally demagnetized, with a few subjected to AF demagnetization. In 28 specimens, a ChRM oriented downward toward the N–NW was isolated between 10 and 15 mT and 50–60 mT (Fig. 6a) or 20–120 °C and 400–440 °C (Fig. 6b). The sample set from the lower part of the section shows clear normal polarity, and normal polarity was also clearly recognized in the sample set located in the upper part (Figs. 6b and 7).

Logs 1, 2 and 4 were investigated for paleomagnetism in the Specchi composite section (Fig. 7c). In the Log 1 (site VE04), most samples display a low-temperature/low-coercivity component of normal polarity, interpreted as a viscous magnetization, and random behavior at higher temperatures or AF levels. In some samples, demagnetization diagrams show a gradual shift toward the southern and upward direction, and in a few cases, a poorly defined reverse-polarity ChRM was identified (Fig. 6g, h). The base (from 0.4 to 1.9 m) and upper part (from 2.4 to 3.4 m) of the section have uncertain polarity because samples analysed using the thermal method showed reverse polarity, while samples analysed using the AF method showed normal polarity. The collected samples from the interval from 1.9 to 2.4 m showed reverse

Table 3
Summary of the biofacies and their features.

Biofacies Code	Biofacies name	Main features
B1	*Ammonia beccarii*	Predominance of epiphytic specimens *Ammonia beccarii, Elphidium crispum* and *Nonion boueanum* as main constituent and common *Ammonia inflata, Cribroelphidium decipiens, E. granosum* and *Fursenkoina schreibersiana* as subordinate constituent. Two sub-biofacies can be recognized: B1a, characterised by sandy or silty vegetated substrate of the inner portion of infralittoral zone; B1b, characterised by muddy-silt in the outer portion of infralittoral zone. These biofacies indicate moderate to high energy setting, normal salinity, well-oxygenation and good light conditions (Murray, 1968, 1991; Poag, 1981). On average the specimen's diversity of these biofacies is tendentially low.
B2	*Ammonia tepida*	Common presence of nominal *taxon* which can be exclusive or with common or rare undersized *A. beccarii,* rare *Aubignyna perlucida and Miliammina fusca*. The ostracod fauna is composed of *Cyprideis torosa*, *Loxoconcha ovulata*, *Xestoleberis plana* and of rare allochthonous valves of *Cypria ophtalmicica*; carbonized vegetal rests and oxides grains are rarely-common recognizable. Washed residues usually are scarce, relating to a muddy or silty mud substrate in a low energy paleoenvironmental setting attributable to a hypoialine lagoon. The undersized dimension of the above-mentioned benthonic foraminifera is typical of salinity condition lower than normal (Walton and Sloan, 1990).
B3	*Nonion boueanum*	Dominance and abundance of the nominal *taxon*, subordinate rare to common *A. perlucida*, very rare *A. tepida, Bolivina* sp., *Bulimina* spp. for benthonic foraminifera; very rare *Globigerinoides* spp. for planktonic foraminifera. This biofacies is characterised also by very abundant echinoid spines, gypsum crystals and very scarce terrigenous fraction. This biofacies is referred to a deposition in the infralittoral zone with low to very low sedimentation rate, in normal saline condition which allows very favorable standard for the proliferation of *N. boueanum* which optimum living condition is in a range depth of 25 to 50 m according to Van Voorthuysen (1973). The faunal assemblage suggests also the presence of poorly oxygenated condition at sea bottom (Diz et al., 2002)
B4	*Buliminids*	Presence of rare to common *Bulimina* spp. and *Bolivina* spp., subordinate species of *Cassidulina, Globobulimina* sp. and *Uvigerina* sp. which according to Gupta and Castillo (1993), Kaiho (1994) and Koho and Piña-Ochoa (2011), are species that live under dysoxic and anoxic conditions. Generally, this biofacies is recognized in sediments characterised by mudstone and silty mudstone with sulfide spherules. The microfaunal association indicates poor bottom oxygenation conditions probably related to the absence or weak circulation of marine currents.
B5	*Miliolids*	Presence of common *Quinqueloculina seminulum*, *Triloculina oblonga*, subordinate *Q. vulgaris* among the miliolids and other shallow-water taxa such as *Ammonia beccarii* and *Nonion boueanum*. This lithofacies refers to a deposition in the infralittoral zone characterised by a sandy bottom. The absence of echinoid remains suggests possible slightly higher salinity conditions.
B6	*Globigerinoides*	Presence of common *Globigerinoides* spp. and diversified association with subordinate *Globigerina* spp. for planktonic foraminifera and shallow-water specimens for benthonic foraminifera.
B7	*Globigerina*	Rare to common *Globigerina* spp. characterised by diversified association, with subordinate *Globigerinella* spp., *Globigerinoides* spp. and *Neogloboquadrina* spp. for planktonic foraminifera; rare benthonic foraminifera may also be present. This biofacies is referred to a deposition in the distal portion of infralittoral to proximal circalittoral zone.
B8	Ostracods	Characterised by a very low diversity in the ostracofaunas, that is composed of rare *Candona* sp., *Cyprideis torosa, Potamocypris* cf. *Potamocypris zschokkei*, ostracod fauna, and gastropod operculum. Carbonized vegetal rests, rare oxides and reworked foraminifera have been recognized. Washed residues of the samples which contain this biofacies is related with a mud or a silty mud sediment, typical of a very low or low-energy depositional setting. Faunal content and lithological features are indicative of lacustrine environment with oligo-mesohaline waters.

(caption on next page)

Plate 2. 1, *Petaloconchus intorsus* (M. Molini - 16 m); 2, *Aphorrais uttingeriana* (M. Molini - 7 m); 3, *Neverita josephinia* (Capaccia - 22 m); 4, *Dendrophyllia* (*cornigera?*) (Montebello - 11.5 m); 5, *Dentalium* sp. (M. Molini - 7 m); 6, *Cerithium* sp. (Spoiano - 14 m); 7, *Bolinus brandaris* (Capaccia - 13 m); 8, *Anadara gibbosa* (M. Molini - 18 m); 9, *Nassarius* sp. (Spoiano - 12 m); 10, *Heliacus* sp. (Capaccia - 13 m); 11, *Bathytoma cataphracta* (Montebello - 10 m); 12, *Euthria cornea* (Montebello - 10 m); 13, *Ocenebra erinaceus* (Ginestra - 14 m); 14, *Solatia* (*hirta?*) (Spoiano - 12 m); 15, *Conus* sp. (Capaccia - 13 m); 16, *Hadriania* sp. (Spoiano - 11 m); 17, *Helminthia vermicularis* (Capaccia - 13 m); 18, *Glycymeris insubrica* (Spoiano - 21 m); 19, *Nassarius* sp. (Spoiano - 12 m); 20, *Venus* sp. (P. Cavallo - 5.5 m); 21, *Glycymeris pilosa* (Capaccia - 13 m); 22, *Pelecyora brocchii* (Spoiano - 11 m); 23, barnacles (Capaccia - 10 mm). White bar is 1 cm.

polarity. In Log 2 (site VE05), 12 samples were collected. After removal of a low-temperature, low-coercivity normal-polarity component, the lower part of the section shows erratic directions, while in the upper part a normal-polarity ChRM was isolated between 20 and 120 °C and 400–440 °C or up to 35 mT (Fig. 6i). In Log 4 (site VE06), all three demagnetized samples display normal polarity.

In the Spoiano section 24 samples were collected for paleomagnetic investigations (Fig. 7d). A well-defined ChRM was isolated in 23 samples up to 80 mT or 440–580 °C (Fig. 6e, f). Among these, 21 samples show ChRMs directed north and downward, indicating deposition during a normal-polarity chron for the interval below the unconformity at ~4.8 m and from ~6 up to ~9.5 m from the base of the section (Fig. 7d).

4.2.2. Magnetic mineralogy

Most samples reached 90% of their saturation magnetization by 100 mT, indicating a dominance of low-coercivity components. Thermal demagnetization of three-component IRMs shows maximum unblocking temperatures of about 580 °C, consistent with magnetite. A smaller number of samples did not reach IRM saturation even at 2.7 T, suggesting a predominance of high-coercivity minerals. Thermal demagnetization of these samples revealed maximum unblocking temperatures around 680 °C, consistent with hematite.

5. Discussion

This chapter discusses the bio- and magnetostratigraphic calibration of the marine and continental succession of the central sector of the Valdelsa Basin, its depositional evolution and the paleoclimatic framework, focusing particularly on the mid Pliocene Warm Period.

5.1. Biostratigraphy

Considering planktic foraminiferal biostratigraphy, a first significant *datum* is the persistent absence of *Globorotalia puncticulata* in all the analysed samples. In fact, the LO (Last Occurrence) of this *taxon* is astronomically calibrated at 3.57 Ma, just before the Zanclean - Piacenzian boundary (Lirer et al., 2019). This allows us to attribute the studied succession to the Piacenzian, supporting previous findings by Capezzuoli et al. (2005). These deposits are also coeval with those of similar successions in the adjacent and westernmost Volterra Basin (Bossio et al., 1994; Costantini et al., 2002; Lazzarotto et al., 2002; Riforgiato et al., 2005) and the southernmost Siena Basin (Bossio et al., 1993b; Martini and Sandrelli, 2015; Martini et al., 2016). The absence of *G. puncticulata* in association with the presence of *Neogloboquadrina planispira* and *Globigerinoides ruber* in the lower part of the succession, constrains the age to no older than the *Globorotalia crassaformis* Subzone (MPL4b), according to the scheme of Lirer et al. (2019). Furthermore, lower sediments of FAA are assigned to an interval spanning the upper MPL4b (*G. crassaformis* Zone) to the top of the MPL4c (G. bononiensis/S. seminulina Sub-Zone). This attribution is based on the occurrence of *G. crassaformis*, *G. bononiensis*, and *S. seminulina* in the lower FAA samples from the central Basin (e.g., San Giorsolè, Volpaia, Cignano, Falisca area of Fig. 2a; section II, S3), consistent with observations from the western sector (Capezzuoli et al., 2005; Milaneschi et al., 2024; Cornamusini et al., 2025). Notably, the first occurrence of *G. crassaformis* is linked to its reappearance at 3.35 Ma (as per Lirer et al., 2019). This is supported by the fact that the lowermost samples of the succession are only slightly older than the Last Occurrence (LO) of *G. puncticulata*.

Furthermore the bio-chronostratigraphic calibration of the upper part of the succession, widely outcropping in the western sectors of the Basin, can be attributed to the *G. bononiensis* Subzone (MPL5a), due to the recognition of the LO of *Sphaeroidinellopsis seminulina* in the lower part of P. Cavallo section (Figs. 4; S2), which marks the top of the *Globorotalia bononiensis/Sphaeroidinellopsis seminulina* Sub-Zone (Lirer et al., 2019). Unfortunately, the very marginal environment characterizing the upper part of the succession did not allow for the identification of biostratigraphically significant elements in the very scarce planktic assemblage recovered.

In addition, among the benthic foraminifera, the occurrence of *Textularia jugosa* in the lowermost samples of the Montebello section, although not conclusive, supports a chronostratigraphic attribution to the Piacenzian, as also indicated by Capezzuoli et al. (2005).

5.2. Magnetostratigraphy

The integration of biostratigraphic with paleomagnetic data allows a reconstruction of a magnetostratigraphic framework, identifying magnetochrones for the P. Cavallo, Specchi composite, Spoiano and M. Molini sections.

In the P. Cavallo section, three polarity intervals were identified: two with reverse polarity and one with normal polarity (Fig. 7). Based on the biostratigraphic data and the zonal scheme of Lirer et al. (2019), the reverse-to-normal transition at the base of the section can be correlated with the C2An.2r (Mammoth subchron) / C2An.2n boundary, dated at 3.207 Ma (Ogg, 2020). Correlation of the normal-polarity interval with subchron C2An.2n is supported, as previously demonstrated, by the absence of Zanclean deposits in the studied succession. Correlation with an older subchron would imply a Zanclean age for the section base, which can be excluded based on stratigraphic evidence. Accordingly, the magnetic reversal at ~16 m is correlated with the C2An.2n / C2An.1r (Kaena subchron) boundary at 3.116 Ma.

This model implies a sedimentation rate of ~16 cm/kyr, calculated from the ages of the two magnetic reversals identified in the P. Cavallo section. This is consistent with the 14 cm/kyr rate estimated by Riforgiato et al. (2011) for Pliocene marine mudstones in the westernmost Fine Basin. Assuming this rate remained approximately constant throughout the middle to upper parts of the section, the C2An.1r / C2An.1n reversal would be expected at around 29 m in the stratigraphic column. However, the uppermost lithologies were not suitable for sampling, preventing confirmation of this hypothesis.

In the Specchi section, paleomagnetic data indicate a probable reverse polarity in Log 1 and a normal polarity in the upper part of Log 2. Based on biostratigraphic data, a reversal from reverse to normal polarity occurs between Log 1 and 2. This reversal can be correlated with the boundary between C2An.2r (Mammoth subchron) and C2An.2n at 3.207 Ma (Ogg, 2020). No paleomagnetic data are available for Log 3, while samples from marine sediments at the top of Log 4 indicate deposition during a normal-polarity interval. Considering that the marine deposits of this interval, belonging to the VLM_2 unit, unconformably overlie those of VLM_1 (upper part of sections I and III), this normal-polarity interval is attributed to subchron C2An.1n, the base of which is dated at 3.032 Ma (Ogg, 2020).

Additional paleomagnetic data were obtained from the M. Molini and Spoiano sections. Four sets of measurements were collected: two from M. Molini (lower and upper parts) and two from Spoiano (below

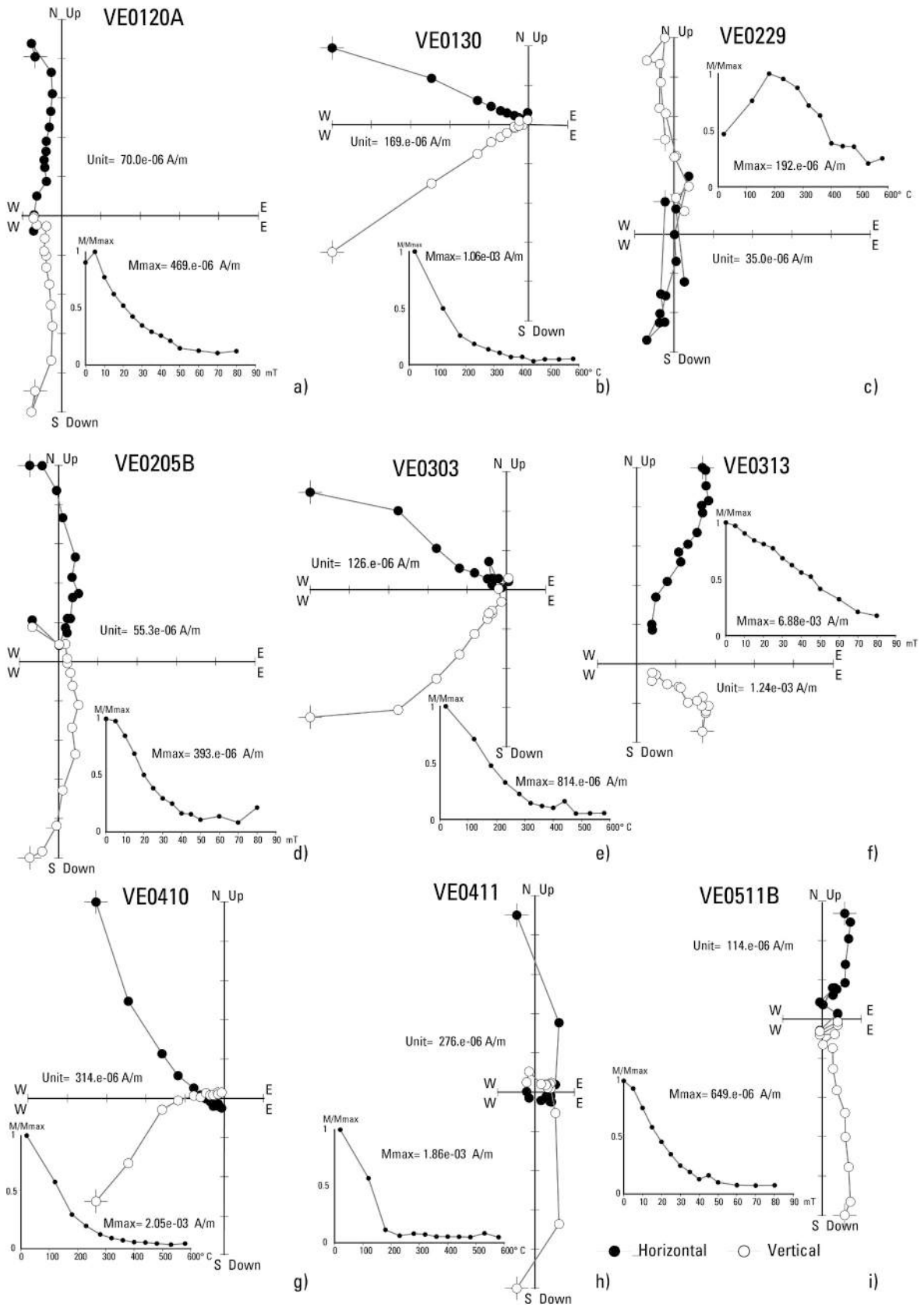

Fig. 6. Zijderveld diagrams: Stereographic plot, Zijderveld diagrams and demagnetization step (normalized intensity of magnetization vs temperature in °C for thermal and mT for Alternating Fields methods) of some representative samples from M. Molini (*a*, *b*), P. Cavallo (*c*, *d*), Spoiano sections (*f*) and Specchi (*g*, *h*, *i*).

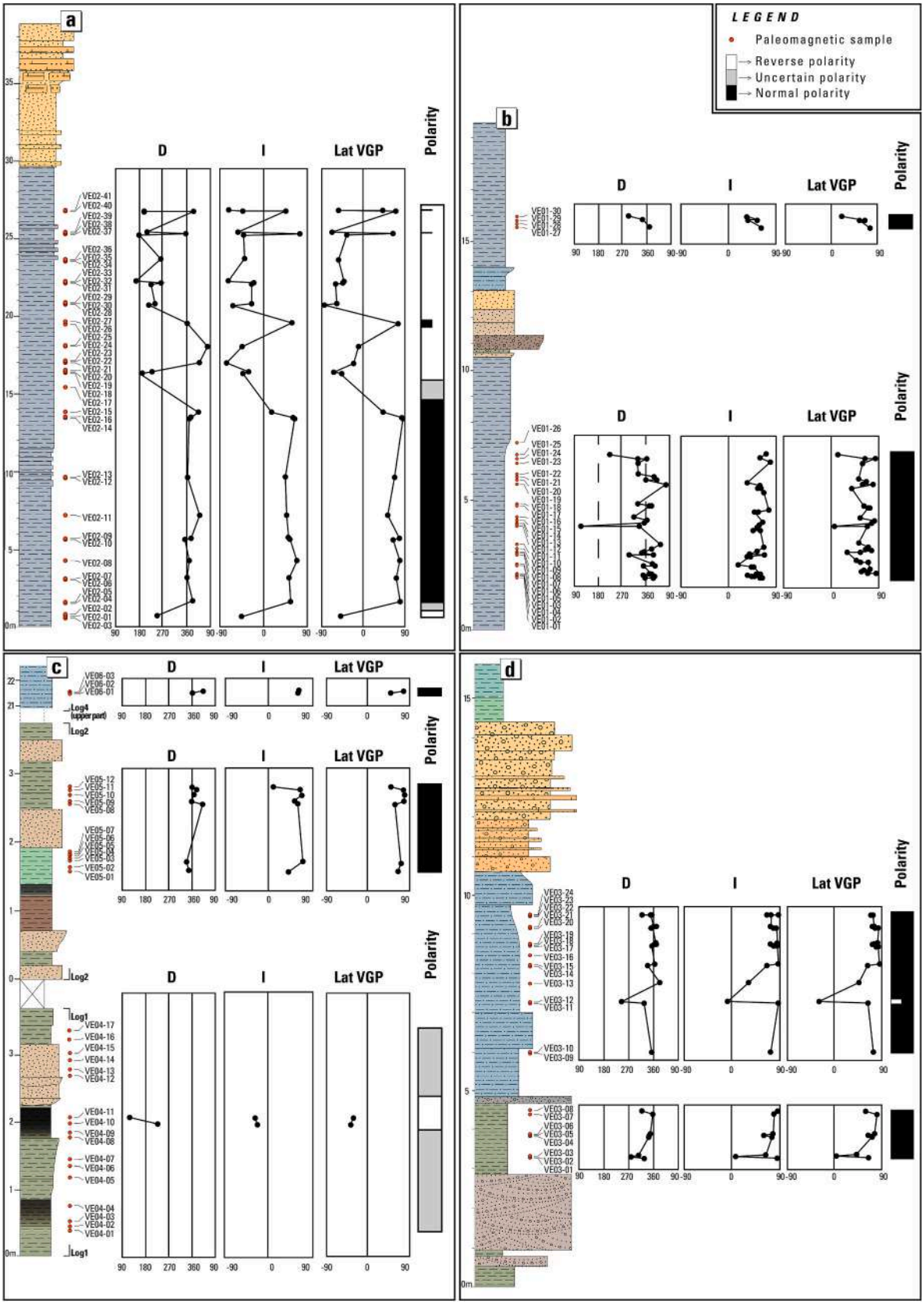

Fig. 7. Polarity: Paleomagnetic results of P. Cavallo (*a*), M. Molini (*b*), Specchi (*c*) and Spoiano (d) sections. The results for declination (D), inclination (I), Visual Geographic Position (VGP) and interpreted polarity are reported. For lithologies see Fig. 4.

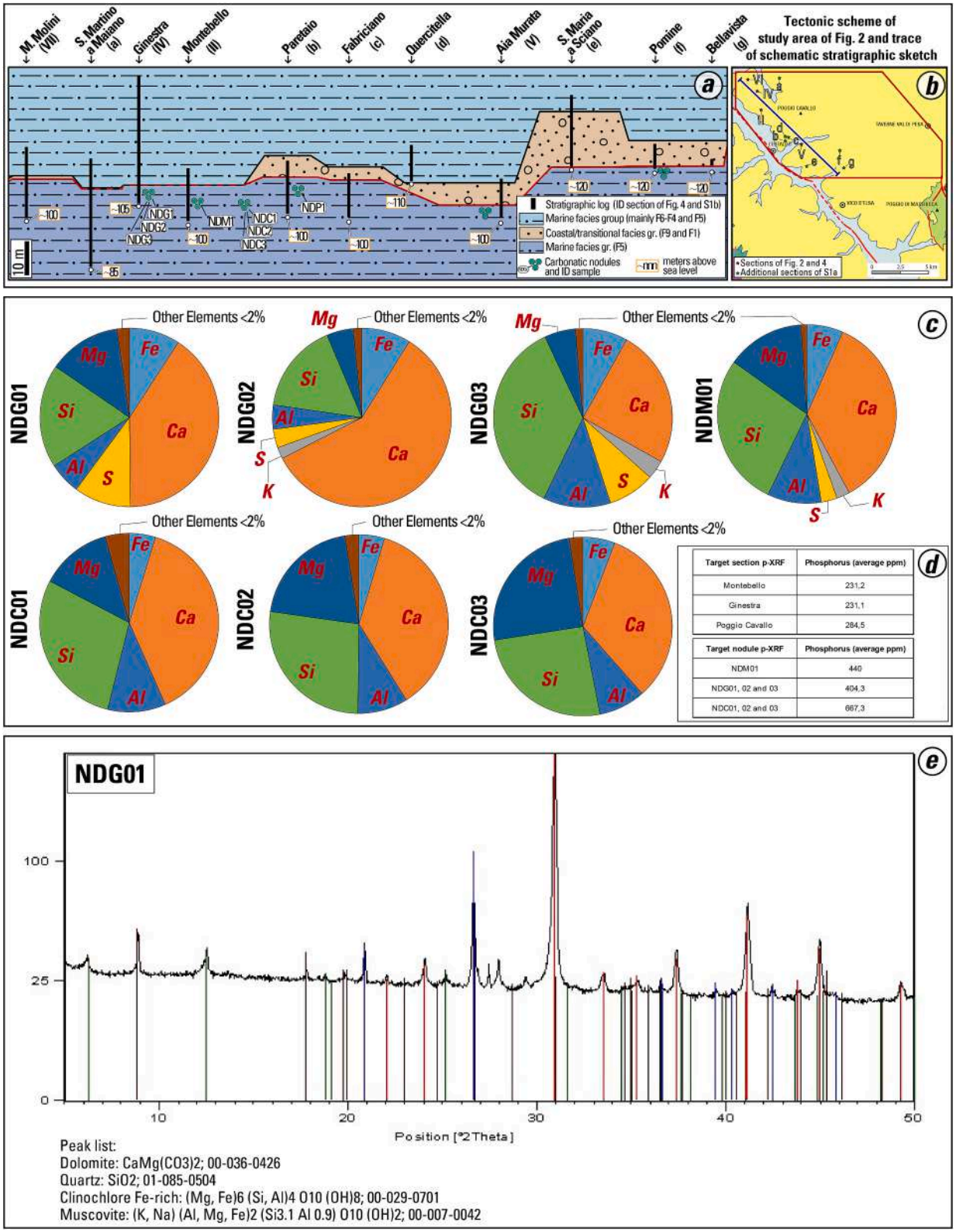

Fig. 8. *a*, Paleoenvironmental correlation sketch of a NW-SE transect of the study area of Fig. 2. Sections reported in Fig. 4 are coded with Roman numbers, while additional sections measured and sampled during the fieldwork are coded with letters. The sketch shows the stratigraphic position of the dolomitic nodules; *b*, Tectonic scheme of the study area showing the trace of the paleoenvironmental correlation sketch. The locations of all the studied sections are shown; *c*, Circular diagrams showing the concentrations of elements exceeding 2% in the carbonate concretions of the Ginestra section (NDG), Montebello (NDM) and Poggio Cavallo (NDC) sections; *d*, average concentration of phosphorus (ppm) in the Montebello, Ginestra and Poggio Cavallo sections, and in the cemented nodules sampled in the same sections; *e*, XRD spectrum of NDG01 nodule of Ginestra section.

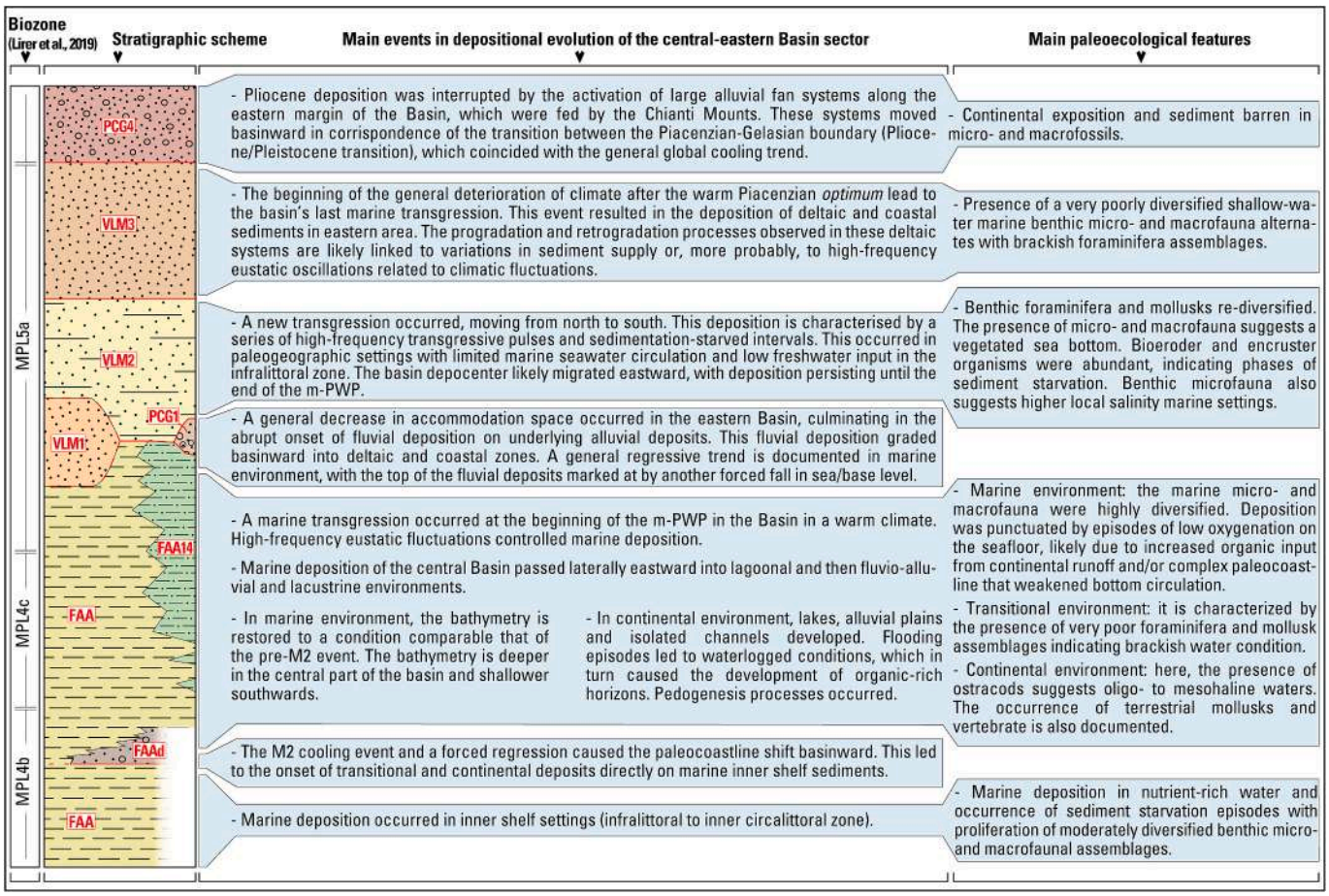

Fig. 9. Summary scheme of the main paleoenvironmental events in the depositional evolution of the studied Valdelsa Basin sector and their respective paleoecological settings. Lithostratigraphic codes are from Fig. 2 and Cornamusini et al. (2025).

and above the Lag facies; Fig. 4d). The results indicate deposition during a normal-polarity chron in both sections. The lower part of the Molini section correlates with subchron C2An.3n, whereas the upper part corresponds to C2An.2n. Both sets of samples from the Spoiano section are attributed to subchron C2An.1n (base at 3.032 Ma; Ogg, 2020), based on correlation with the other studied sections.

5.3. Paleoenvironmental settings and depositional evolution

The main events recognized during the depositional evolution of the studied area, along with their respective paleoecological settings, are reported below and summarised in Fig. 9.

The depositional history of the studied succession of the Valdelsa Basin begins with the Argille Azzurre (FAA), which testifies a marine deposition spanning the distal infralittoral to the proximal circalittoral zone in an interval attributable to the upper part of MPL4b (Fig. 5). The micro- and macropaleontological assemblages, particularly the filter-feeding and gregarious organisms, indicate the occurrence of conditions rich in high-nutrient with low sedimentation rate. The first change in the sedimentary style is represented by the deposition of the FAA_d horizon (Figs. 2, 3 and 5), characterised by coarse-grained facies deposited in coastal-deltaic to continental environments, mainly composed of the F9 and F1 facies associations (log V and VI of Fig. 5). FAA_d, which exhibits a lenticular geometry at a constant altitude of 120 m a.s.l. (Fig. 8a), records an important depositional shift in the Basin. This shift leads to the deposition of transitional and continental deposits above inner shelf mudstone in the Basin depocenter's.

The paleocoastline in the Certaldo area, trending SE-NW, primarily received clastic input from fluvial systems, draining from the eastern Tavarnelle-Montespertoli High (Fig. 2b). In NW sectors of the study area, FAA_d has not occurred and is replaced by a discontinuous layer of dolomitic nodules interbedded in F6 (Figs. 2, 5 and 8a), suggesting the presence of a complex coastal paleogeography, characterised by gulfs and bays. While some areas were reached by coastal and deltaic systems, others remained submerged in shallow-water settings, consistently maintaining a bathymetry within the proximal infralittoral zone.

Chemical and mineralogical analyses of these nodules (Fig. 8c, e) reveal a primary composition of dolomite and a significantly higher phosphorus content (~400–700 ppm, Fig. 8d) compared to the average of all other samples (~200 ppm). Although this phosphorus concentration is not high enough to form phosphorite, the genesis of the nodules can be related to a sedimentation stasis event or a phase with low sedimentation rate, likely associated with a relative sea-level rise (Föllmi et al., 1991). The genesis and dolomitic composition of these nodules are attributable to post-depositional processes. These nodules are commonly found below the F9 facies association or below fossil-rich sandy matrix concentrations. The higher permeability of these coarse-grained or fossiliferous horizons allowed fluids, rich in high-Mg calcite, to percolate into the underlying mudstone, and to promote the formation of the dolomitic horizon.

Above FAA_d, a transgressive phase started in the depocentral sectors of the Valdelsa Basin, likely in correspondence to the interglacial stage M1 (Fig. 5). This is evidenced by the presence of marine sediments overlying coastal and fluvial facies deposits in the Certaldo area. Biofacies distribution analysis shows that in the Ginestra and lower P. Cavallo sections (Fig. 5), the marine transgression led to the development of a deep infralittoral zone within the northwestern sector. Concurrently, in the southeastern sectors, sedimentation occurred in the

proximal part of the infralittoral zone to coastal environments, characterised by poorly diversified assemblages. As the transgression advanced, deposition occurred in progressively deeper environments from the distal infralittoral up to the proximal circalittoral zone. The micropaleontological analysis indicates a rapid evolution in the faunal assemblages, with an increase in species diversity and numbers of individuals.

During the first ~200 kyr of the middle Piacenzian *optimum*, the Valdelsa basin was characterised by high-frequency sea level fluctuation, as evidenced by the biofacies stacking analysed among the recognized facies association. In general, the foraminiferal assemblages were dominated by benthic rather than planktonic foraminifera. Planktonic foraminifera, are mainly represented by *Globigerinoides* genus (*G. ruber*, *G. elongatus* and *G. trilobatus* among others), typical superficial water species (Bé et al., 1977; Darling et al., 1999; Kucera, 2007), suggesting a settlement of deposition in protected bays or gulfs (Tolderlund and Bé, 1971). Furthermore, the marine deposition has also been punctuated by episodes of under-oxygenated seafloor settings. This is suggested by the presence of B3 and B4 biofacies in the upper part of the Argille Azzurre, which are characterised by taxa that thrives in suboxic and dysoxic conditions (Kaiho, 1994). The local presence of vermetids and scaphopods concentrations indicates episodes of sedimentation stasis, which allowed these gregarious organisms to proliferate. In addition, the presence of very rare glauconite grains and glauconitized foraminifera suggests episodes of starvation during sedimentation (Odin and Matter, 1981). While these glauconitic granules are commonly documented in deep marine settings, they can also occur in shallower environments like estuaries and coastlines (Amorosi, 1997; Banerjee et al., 2016). The presence of glauconite, along with bryozoans, bivalves, and other heterotrophic filter-feeders organisms, reflects conditions of high nutrient concentration.

At the beginning of the warming phase of the mid-Pliocene's climatic *optimum*, sedimentation in the eastern sector of the Valdelsa Basin was predominantly continental and transitional in environment. This is evidenced by the thick floodplain, fluvial, lacustrine, and lagoonal deposits (Rio Apoli member - FAA_{14}), and supported by facies and ostracod fauna analyses, as well as previously recorded by Aldinucci et al. (2019). In this continental interval, floodplain mudstone are locally incised by small, isolated (ribbon-like) channels and are also characterised by the presence of dark, organic-rich horizons, which document the onset of a high-water table linked to a relative base-level rise. Consequently, these features can be interpreted as the expression of flooding surfaces within a broader transgressive system tract context, indicating an increase in accommodation space (Wright and Marriott, 1993; Einsele, 2000). The dynamics of accommodation space in the upper part of this continental succession have been also documented by Aldinucci et al. (2019). In the Specchi area, these authors identified the replacement of ribbon-like channels by amalgamated ones upward the succession. According to their study, this transition reflects a decreasing trend in accommodation space, which culminated to the emplacement of the F2 fluvial conglomerates in Specchi and Spoiano areas (Specchi Member - PCG_1) unconformably overlying the Rio Apoli Member (FAA_{14}). Indeed, the continental deposition graded into lagoonal and then to marine sediments basinward (Fig. 5). This is demonstrated by the brackish microfauna of the B2 biofacies, recognized in samples from the Luia section (Fig. 5) in the Agliena Creek valley, and is consistent with findings proposed by Aldinucci et al. (2019). The presence of brackish microfauna, recognized in the lagoonal facies (F7) of this section, can be probably correlated with the onset of lacustrine settings (F3 facies association) in the middle-lower part of the Log 4 of Specchi. Just below this lacustrine facies deposits, the dark horizon of Cm2 facies has been certainly correlated with ones recognized in the lower part of the Capaccia section according to Benvenuti et al. (2021). Subsequently, a new rapid transgression occurred, which led to the sedimentation of the sandy marine deposits of the Podere Capaccia member (VLM_2) (Figs. 2 and 5). The marine deposition of the sandy F5 facies association, identified in the Capaccia and Spoiano sections as well as in the upper part of Log 4 of Specchi, occurred within the infralittoral zone on a sandy and vegetated seafloor. This deposition is characterised by a series of transgressive phases and sedimentation-starved intervals, as evidenced by fossil-rich concentrations (Fig. 5), most likely linked to high-frequency eustatic fluctuations. In addition, the presence of pervasive bioeroder and encruster organisms in these deposits supports the occurrence of events with a low sedimentation rate (Bromley and D' Alessandro, 1983; Galinou-Mitsoudi and Sinis, 1995), which allow benthic communities to proliferate in shallow-water settings. The occurrence of the B5 biofacies in these sections, with their dominant miliolids and absence of echinoid remains, suggests that this marine environment experienced episodes of salinity conditions higher than normal (Haq and Boersma, 1998; Murray, 2006). These conditions are indicative of paleogeographic settings characterised by limited marine seawater circulation and low freshwater input. To explain the variation in the thickness of the VLM_2 member in Capaccia (~18 m thick) and Spoiano (~5 m thick) sections (Fig. 5), where in both F5 facies association are present, the following hypotheses can be considered: *i)* the VLM_2 unit was deposited diachronously, with a transgressive front moving from north-west to south-east. This was likely controlled by a topographic high in the Spoiano area, which was only later inundated by marine facies; *ii)* the VLM_2 sediment in the Spoiano area was eroded more extensively due to the onset of the overlying VLM_3 unit. Taking these hypotheses into account, the first is more reliable, although the lack of sediment thickness in each section due to the presence of an erosive surface at the top of VLM_2 cannot be excluded. The top of the VLM_2 marine deposits is separated by an erosional surface from the sediments of the Semifonte member (VLM_3), which outcrops with a thickness of approximately 50 m at Capaccia section. The onset of the VLM_3 proximal delta front in alternation with F5 shallow-water marine facies associations evidence high-frequency oscillations, indicating progradation and retrogradation of the deltaic systems, punctuated by higher energy episodes as suggested by the presence of large brackish mud clasts. During the deposition of VLM_3 unit, we assists to a general deepening of the succession which pass from deltaic condition upward to lagoonal to shallow-water marine (F7 to F5 in Capaccia) and lacustrine to lagoonal (F3 to F7 occur in Spoiano). Only in Capaccia section, after another consistent erosion marked with the emplacement of fluvio-alluvial deposits (F10), the final shallow-water marine deposition occurs (F5 and F4 alternation), abruptly eroded by the coarse-grained alluvial conglomerate of PCG_4 (Fig. 5). The emplacement of coarse PCG_4 coarse deposits attests the progradation of alluvial and fluvial-alluvial systems from the Chianti Mountains toward the depocenter and the western sectors of the Valdelsa Basin at the Plio-Pleistocene transition (Canuti et al., 1966; Benvenuti et al., 2014; Aldinucci et al., 2019).

5.4. Paleoclimatic framework

The obtained chronological framework and the comparison with the LR04 benthic stack (Lisiecki and Raymo, 2005), also scaled to global eustatic sea level according to Miller et al. (2012), allowed the identification of specific global climatic events as the primary drivers of sedimentary responses and environmental changes in the Basin. It's worth considering that in such a narrowed basin, characterised by marginal continental, transitional and shallow-water marine environments, small-scale sea level fluctuations can produce significant shifts in depositional systems.

In the lower part of the studied succession, the abrupt onset of the FAA_d transitional and continental deposits of directly over FAA inner shelf mudstone, coupled with biofacies stacking pattern indicating a rapid decrease in bathymetry (section II and VI, Fig. 5), can be correlated with the M2 sea-level fall event at ~3.3 Ma (Fig. 5). This cold climate event, according to the LR04 curve, caused a negative sea-level fluctuation of approximately −60 m, marking the base of the Piacenzian *optimum* (Mudelsee and Raymo, 2005; Miller et al., 2012; Dolan et al.,

2015). The first ~200 ~250 kyr after the M2 marine isotope stage is a key interval in the Pliocene climate, because it is characterised by benthic foraminiferal isotopic values that are lighter than or equal to those observed today, with the exception of the KM2 glacial stage (Lisiecki and Raymo, 2005; Dowsett et al., 2021). This time period is widely studied for its paleoenvironmental, paleogeographic, and geochemical proxy data, which are very important for paleoclimatic reconstructions (Dowsett et al., 1994, 1996, 2016, 2021; Haywood et al., 2016, 2021).

During the first ~250 kyr of the middle Piacenzian *optimum*, the Valdelsa Basin was characterised by high-frequency sea level fluctuation, as evidenced by the biofacies stacking pattern analysed among the facies association (e.g. the shallow-deep alternation of section I, Fig. 5). The presence in this interval of faunal assemblages characterised by *Globigerinoides* spp. (B6 biofacies, Fig. 5) among planktonic and benthic taxa which thrive in suboxic and dysoxic conditions (B3 and B4 biofacies, Fig. 5), suggests a deposition in warm-water punctuated by episodes of under-oxygenated seafloor settings. The onset of depleted-oxygen conditions on the seafloor, also indicated by the local presence of sulphur spherules, was probably linked with increased precipitation during warm, humid phases, resulting in increased superficial runoff. The resulting increase in freshwater input to the basin, as evidenced by carbonized plant remains in the marine facies (see Table 1), would introduce higher levels of organic matter and nutrients in the sea water. This would weaken the ventilation at the seafloor, which is induced by superficial water stratification (Rossignol-Strick, 1983; Rohling, 1994). The hypothesis that climatic forcing triggered the local onset of oxygen-depleted conditions is supported by the intermittent nature of the related biofacies throughout the succession. If restricted marine circulation was primarily controlled by the basin's physiography - which remained stable during the studied interval - the effects on the benthic assemblages would be continuous and permanent. Instead, the local presence of brachiopods (e.g. in the upper part of Montebello section, II in Fig. 5), suggest episodes of well-oxygenated, warm-water conditions (García-Ramos et al., 2020).

During the deposition of the marine mudstone (FAA), the two sandy intercalations present in P. Cavallo, which occurred after the LO of *Sphaeroidinellopsis seminulina* and the magnetic inversion in the middle part of the section (see Fig. 5), are probably correlated with the KM2 and G22 cold stages of the LR04. These cold phases may have likely triggered the relative falls in the sea level and the subsequent progradation of fluvial systems in the eastern area, which accumulated a higher detrital input in the area of the section.

The disconformity occurring between VLM_2 and VLM_3 was most likely caused by climatic factors, with the sea-level fall correlated with the G10 phase at 2.8 Ma (Fig. 5). This negative eustatic fluctuation would have led to the onset of sediments of VLM_3, consisting of deltaic deposits, mainly proximal delta front coarse sandstones, lying on bluish very fine sandstones of VLM_2. In the first phases of the VLM_2 deposition the high-frequency fluctuations shown in the LR04 can be responsible for the stacking of fining upward trend set, each one marked by a fossiliferous horizon at the base, present in Capaccia section (Fig. 5). Upward, with the onset of VLM_3, the alternations of sandy and pelitic sediments (F5/F8) in the Capaccia section, from approximately 25 to 35 m, testify the progradation and retrogradation processes of a deltaic system in this part of the Basin, likely linked with high-frequency eustatic oscillations related to climatic fluctuations.

The abrupt onset of proximal deltaic facies at the base and in the middle part of VLM_3 (Fig. 5), are probably correlated with glacial stages G10 and G6. Indeed, the high frequency fluctuations recorded by the facies association stacking in Capaccia and Spoiano sections between these two cold phases (Fig. 5), are consistent with the $\delta^{18}O$ trend reported by Lisiecki and Raymo (2005). At the top of the Capaccia section, coinciding with the transition interglacial stage G1 to MIS 104 and the overall climatic cooling at the Pliocene-Pleistocene boundary, we observe the emplacement and basinward progradation of the large PCG_4 alluvial and fluvial-alluvial systems from the Chianti Mountains (Figs. 2 and 5). This event marked the end of the Plio-Pleistocene succession at Basin scale.

6. Conclusions

The application of an integrated multiproxy methodological approach allowed for a detailed bio-, magneto-, chronostratigraphic calibration and chronology of the Valdelsa Basin Pliocene succession, enabling a redefinition of the stratigraphic architecture and providing new insights into its paleoenvironmental and paleoclimatic evolution, particularly during and around the mid-Pliocene Warm Period. Facies analysis allowed the identification of ten distinct facies associations, which were then categorised into continental, transitional, and shallow-water marine environments. These facies collectively form an articulated stratigraphic architecture, reflecting the depositional response to Piacenzian sea-level fluctuations driven mainly by climatic variations. The high-resolution stratigraphy of the studied succession, defined by new biostratigraphic and magnetostratigraphic data, frames it within the interval spanning the upper part of the *G. crassaformis* Subzone (MPL4b) and the *G. bononiensis* Subzone (MPL5a). Additionally, two magnetic inversions were detected: C2An.2r/C2An.2n and C2An.2n/C2An.1r. Facies analysis, combined with new age constraints, suggest that marine deposition in the Valdelsa Basin during Zone MPL4b was abruptly interrupted and replaced, through an erosional surface, by coastal and continental deposits, which lie disconformably on to inner shelf deposits, in correspondence with the isotope marine stage M2 at ~3.3 Ma. Subsequently, with the onset of the general warming phase that characterised the Piacenzian climatic *optimum*, a new transgressive phase occurred in the Valdelsa Basin, likely started during the M1 interglacial phase, with a deposition that span up to the lower part of MPL5a. This phase was characterised by high-frequency eustatic oscillations and diversified micro- and macrofauna, indicating bathymetries ranging from the infralittoral to the proximal circalittoral zones and indicative of warm, nutrient-rich waters characterised by episodes of sedimentary starvation, proliferation of benthic organisms and depleted-oxygen conditions event at seafloor. While marine sediments were mainly deposited in the central areas of the Valdelsa Basin, the central-eastern sectors (Pesa sub-basin) experienced the development of alluvial plains with episodes of waterlogging conditions, leading to the formation of organic-rich horizons alternating with pedogenesis and fluvial incision, in response to the fluctuation of the water table. Following the forced incision of fluvial systems into muddy alluvial plain deposits, which graded basinward into deltaic and coastal sandstone, a new transgression occurred. This event was characterised by shallower water depths than previous transgression, remaining within the inner infralittoral zone. This phase, according to the chronostratigraphic framework, occurred during the middle part of Zone MPL5a and was also characterised by high-frequency eustatic oscillations. After another subsequent fall base-level, a new and last transgressive phase occurred in the Valdelsa Basin during the upper part of Zone MPL5a. This phase involved the deposition of coastal, deltaic, and subordinately lagoonal and continental sediments, which display geometrical relationships related to eustatic fluctuation and variation in sediment supply. Collectively, these last two phases of marine transgression occurred during a general regressive trend, culminating in the emplacement and the basinward progradation of deltaic to fluvio-alluvial systems at the top of the whole succession. This is realised in correspondence with the Piacenzian–Gelasian transition and the general climatic deterioration toward colder temperatures that characterised the Pliocene–Pleistocene transition. With the new stratigraphic framework and by comparing the expanded succession, deposited within the Piacenzian *optimum*, with global benthic $\delta^{18}O$ records (LR04 stack), we identified the main global climatic events driving the depositional evolution in the Valdelsa Basin have been identified. The proposed model reveals a predominance of eustatic control on sedimentation and biofacies distribution, suggesting

that climatic forcing has played a significant role in the development of depositional systems. These new high-resolution data, obtained by an integrated multiproxy methodologies, significantly refine the knowledge of depositional evolution during Piacenzian of the Valdelsa Basin, providing crucial insights for understanding the evolution of Neogene basins within the hinterland of the Northern Apennines during the m-PWP and a comparison tool for similar circum-Mediterranean basins.

Supplementary data to this article can be found online at https://doi.org/10.1016/j.palaeo.2026.113744.

Supplementary paleomagnetic data are available at this link: https://dataservices.gfz-potsdam.de/panmetaworks/review/7773e224e4b1ecde548f26484d3d3ca7ce19de4908f63a7fa578257f0c87a451/

CRediT authorship contribution statement

L. Milaneschi: Writing – original draft, Visualization, Methodology, Investigation, Formal analysis, Data curation, Conceptualization. **G. Cornamusini:** Writing – review & editing, Supervision, Project administration, Funding acquisition. **P. Conti:** Writing – review & editing. **I. Martini:** Writing – review & editing, Supervision, Resources, Data curation. **J. Maffei:** Investigation, Data curation. **F. Cifelli:** Writing – review & editing, Methodology, Investigation, Funding acquisition, Formal analysis. **M. Mattei:** Writing – review & editing, Validation, Methodology, Investigation, Formal analysis. **S. Da Prato:** Formal analysis. **M.C. Alçiçek:** Investigation. **L.M. Foresi:** Writing – review & editing, Validation, Resources, Methodology, Investigation, Formal analysis, Data curation, Conceptualization.

Declaration of competing interest

The authors declare that they have no known competing financial interests or personal relationships that could have appeared to influence the work reported in this paper.

Acknowledgements

We thank the Editor Mary Elliot and two anonymous reviewers for their constructive comments, which significantly improved the quality of the manuscript. This research has been developed within the Italian National Geological and Geothematic Mapping Project – CARG 286-Poggibonsi Sheet (agreement between the Italian Institute for Environmental Protection and Research - ISPRA, the Tuscany Region, and the Department of Physical, Earth and Environmental Sciences- DSFTA of the University of Siena; P.I. Gianluca Cornamusini). Paleomagnetic analyses were supported by the WP3 ILGE - MEET project (PNRR - NextGenerationEU, MUR grant No. D53C22001400005; P.I. Lorenzo Milaneschi). The study was also partially funded by the European Union - NextGenerationEU, Mission 4 Component 1 PRIN 2022 "PPT Impact - Climatic impact on terrestrial and marine realms of the eastern Mediterranean at the Plio-Pleistocene transition" (CUP B53D23006880006; P.I. Ivan Martini).

Data availability

The authors confirm that all data necessary for supporting the scientific findings of this paper have been provided.

References

AGIP Mineraria, 1982. Foraminiferi padani. (terziario e quaternario). atlante iconografico e distribuzione stratigrafica, II edizione (Milano, 52 tav).
Aldinucci, M., Benvenuti, M., Andreetta, A., Dominici, S., Foresi, L.M., Carnicelli, S., Martini, I., 2019. Composite sequence stratigraphic patterns in alluvial to shallow-marine successions: examples from the piacenzian of the valdelsa basin (Central Italy). Sediment. Geol. 388, 99–113.
Amorosi, A., 1997. Detecting compositional, spatial, and temporal attributes of glaucony: A tool for provenance research. Sediment. Geol. 109 (1–2), 135–153.
Athersuch, J., Horne, D.J., Whittaker, J.E., 1989. Marine and brackish water ostracods. In: Kermack, D.M., Barnes, R.S.K. (Eds.), Synopses of the British Fauna (New Series), 43. Brill E.J., Leiden, pp. 1–343.
Banerjee, S., Bansal, U., Thorat, A.V., 2016. A review on palaeogeographic implications and temporal variation in glaucony composition. J. Palaeogeogr. 5, 43–71.
Bé, A.W., Hemleben, C., Anderson, O.R., Spindler, M., Hacunda, J., Tuntivate-Choy, S., 1977. Laboratory and field observations of living planktonic foraminifera. Micropaleontology 155–179.
Benvenuti, M., Del Conte, S., Scarselli, N., Dominici, S., 2014. Hinterland basin development and infilling through tectonic and eustatic processes: latest Messinian-Gelasian Valdelsa basin, northern Apennines, Italy. Basin Res. 26 (3), 387–402.
Benvenuti, M., Andreetta, A., Huertas, A.D., Carnicelli, S., 2021. Palaeosols in an upper pliocene fluvial to shallow marine succession (valdelsa basin, Central Italy): a sequence-stratigraphic perspective. Palaeogeogr. Palaeoclimatol. Palaeoecol. 584, 110684.
Boccaletti, M., Sani, F., 1998. Cover thrust reactivations related to internal basement involvement during Neogene-Quaternary evolution of the northern apennines. Tectonics 17 (1), 112–130.
Bonaduce, G., Ciampo, G., Masoli, M., 1975. Distribution of ostracoda in the adriatic sea. Pubblicazione Stazione Zoologica di Napoli 40, 1–304.
Bonini, M., Sani, F., 2002. Extension and compression in the northern apennines (Italy) hinterland: evidence from the late Miocene-Pliocene Siena-Radicofani basin and relations with basement structures. Tectonics 21 (3), 1–32.
Bossio, A., Mazzei, R., Salvatorini, G., Sandrelli, F., 1993a. Nuovi dati sui depositi Mio-Pliocenici del settore meridionale del bacino del fiume elsa. Paleopelagos 3, 97–108.
Bossio, A., Costantini, A., Lazzarotto, A., Liotta, D., Mazzanti, R., Mazzei, R., Salvatorini, G., Sandrelli, F., 1993b. Rassegna delle conoscenze sulla stratigrafia del neoautoctono toscano. Mem. Soc. Geol. It. 49, 17–98.
Bossio, A., Mazzanti, R., Mazzei, R., Pascucci, V., Salvatorini, G., Sandrelli, F., 1994. Il bacino di volterra: notizie preliminari sullevoluzione della sua area centro meridionale durante il pliocene. Studi Geol. Camerti 1, 19–31.
Bossio, A., Mazzei, R., Salvatorini, G., Sandrelli, F., 2002. Geologia dellarea compresa tra siena e poggibonsi ("bacino del casino"). Atti Soc. Toscana Sci. Nat. Mem. A 107, 69–86.
Brogi, A., 2011. Bowl-shaped basin related to low-angle detachment during continental extension: the case of the controversial neogene Siena basin (Central Italy, Northern Apennines). Tectonophysics 499 (1–4), 54–76.
Bromley, R.G., D' Alessandro, A., 1983. Bioerosion in the pleistocene of southern Italy: Ichnogenera caulostrepsis and maeandropolydora. Riv. Ital. Paleontol. Stratigr. 89 (2), 283–309.
Canuti, P., Pranzini, G., Sestini, G., 1966. Provenienza ed ambiente di sedimentazione dei ciottoli del Pliocene di San Casciano (Firenze). Mem. Soc. Geol. It. 5, 340–364.
Capezzuoli, E., Foresi, L.M., Salvatorini, G., Sandrelli, F., 2005. New data on the middle pliocene sedimentation in the southern Valdelsa Basin (Siena, Italy). Boll. Soc. Geol. It. 4 (10), 95–103.
Capezzuoli, E., Gandin, A., Sandrelli, F., 2006. Depositional and palaeoecological features of the Middle Pliocene (Piacenzian) marine carbonates exposed in the Valdelsa Basin (San Gimignano, Siena, Italy). Geoacta 5, 97–112.
Carmignani, L., Decandia, F., Disperati, L., Fantozzi, P.L., Lazzarotto, A., Liotta, D., Oggiano, G., 1995. Relationship between the tertiary structural evolution of the Sardinia-Corsica-Provençal domain and the Northern Apennines. Terra Nova 7 (2), 128–137.
Catuneanu, O., 2022. Principles of Sequence Stratigraphy. Elsevier Science, p. 494.
Chadima, M., Hrouda, F., 2006. Remasoft 3.0 a user-friendly paleomagnetic data browser and analyzer. Trav. Geophys. 27, 20–21.
Cita, M.B., 1983. Micropaleontologia. Cisalpino Goliardica, Milano, Italy.
Conti, P., Conticelli, S., Cornamusini, G., Marroni, M., 2022. Guide Geologiche Regionali Toscana. Guide Geologiche Regionali, p. 375.
Cornamusini, G., Conti, P., Foresi, L.M., Maffei, J., Martini, I., Milaneschi, L., Tavarnelli, E., 2025. Note Illustrative della Carta Geologica d'Italia a scala 1:50.000 "Foglio 286 Poggibonsi". ISPRA – Serv. Geol. d'It., Roma, p. 258.
Costantini, A., Lazzarotto, A., Mazzanti, R., Mazzei, R., Salvatorini, G., Sandrelli, F., 2002. Note Illustrative della Carta Geologica d'Italia alla scala 1:50.000 "Foglio 285 - Volterra". Servizio Geologico d'Italia, Roma, p. 149.
Dainelli, G., Videssot, P., 1930. Il mare pliocenico nella Toscana settentrionale. Mem. Geol. e Geograf. 1, 125–214.
Darling, K.F., Wade, C.M., Kroon, D., Brown, A.J.L., Bijma, J., 1999. The diversity and distribution of modern planktic foraminiferal small subunit ribosomal RNA genotypes and their potential as tracers of present and past ocean circulations. Paleoceanography 14 (1), 3–12.
Diz, P., Francés, G., Pelejero, C., Grimalt, J.O., Vilas, F., 2002. - The last 3000 years in the Ría de Vigo (NW Iberian Margin): climatic and hydrographic signals. The Holocene 12 (4), 459–468.
Dolan, A.M., Haywood, A.M., Hunter, S.J., Tindall, J.C., Dowsett, H.J., Hill, D.J., Pickering, S.J., 2015. Modelling the enigmatic late pliocene glacial event—marine isotope stage m2. Global Planet. Change 128, 47–60.
Dominici, S., Mazzanti, R., Nencini, C., 1995. Geologia dei dintorni di san miniato tra lArno, lElsa e lEra. Quad. Mus. St. Nat. di Livorno Suppl. 1, 1–35.
Dominici, S., Conti, C., Benvenuti, M., 2008. Foraminifer communities and environmental change in marginal marine sequences (Pliocene, Tuscany, Italy). Lethaia 41 (4), 447–460.
Dowsett, H., Thompson, R., Barron, J., Cronin, T., Fleming, F., Ishman, S., Poore, R., Willard, D., Holtz Jr., T., 1994. Joint investigations of the middle pliocene climate i: prism paleoenvironmental reconstructions. Glob. Planet. Change 9, 169–195.
Dowsett, H., Barron, J., Poore, R., 1996. Middle pliocene sea surface temperatures: a global reconstruction. Mar. Micropaleontol. 27 (1–4), 13–25.

Dowsett, H.J., Robinson, M.M., Haywood, A.M., Hill, D.J., Dolan, A.M., Stoll, D.K., Chan, W., Abe-Ouchi, A., Chandler, M., Rosenbloom, N.A., Otto-Bliesner, B.L., Bragg, F.J., Lunt, D.J., Foley, K.M., Riesselman, C.R., 2012. Assessing confidence in pliocene sea surface temperatures to evaluate predictive models. Nat. Clim. Change 2 (5), 365–371.
Dowsett, H., Dolan, A., Rowley, D., Moucha, R., Forte, A.M., Mitrovica, J.X., Pound, M., Salzmann, U., Robinson, M., Chandler, M., Foley, K., Haywood, A., 2016. The PRISM4 (mid-Piacenzian) paleoenvironmental reconstruction. Clim. Past 12 (7), 1519–1538.
Dowsett, H., Robinson, M.M., Stoll, D.K., Foley, K.M., Johnson, A.L.A., Williams, M., Riesselman, C.R., 2021. The PRISM (pliocene palaeoclimate) reconstruction: time for a paradigm shift. Philos. R. Soc. A 371, 10–1098.
Einsele, G., 2000. Sedimentary Basins: Evolution, Facies, and Sediment Budget, p. 792.
Föllmi, K.B., Garrison, R.E., Grimm, K.A., 1991. Stratification in phosphatic sediments: Illustrations from the neogene of Central California. In: Cycles and Events in Stratigraphy, pp. 492–507.
Galinou-Mitsoudi, S., Sinis, A.I., 1995. Age growth of lithophaga lithophaga (linnaeus, 1758) (bivalvia: Mytilidae), based on annual growth lines in the shell. J. Moll. Stud. 61, 435–453.
García-Ramos, D., Ćorić, S., Joachimski, M., Zuschin, M., 2020. The environmental factors limiting the distribution of Shallow-Water terebratulid brachiopods. Paleobiology 46 (2), 193–217.
Giannelli, L., Mazzanti, R., Mazzei, R., Menesini, E., Salvatorini, G., 1981. Le cave di Poggibonsi e di Castelfiorentino nel quadro del Pliocene della Val d'Elsa. IX Conv. Soc. Pal. It, Pisa, pp. 175–194.
Gupta, B.K.S., Castillo, M.L., 1993. Benthonic foraminifera in oxygen-poor habitats. Mar. Micropaleontol. 20 (3–4), 183–201.
Haq, B.U., Boersma, A., 1998. Introduction to Marine Micropaleontology. Elsevier Eds, p. 384.
Haywood, A.M., Dowsett, H.J., Dolan, A.M., 2016. Integrating geological archives and climate models for the Mid-Pliocene Warm Period. Nat. Commun. 7 (1), 10646.
Haywood, A.M., Dowsett, H.J., PlioMIP1 and PlioMIP2 Participants, 2021. Pliomip: The Pliocene Model Intercomparison Project, 29(2). Past Global Changes Magazine, pp. 92–93.
Holland, S.M., 2023. The contrasting controls on the occurrence of fossils in marine and nonmarine systems. Soc. Pal. It. 62 (1), 1–25.
Holz, M., Kalkreuth, W., Banerjee, I., 2002. Sequence stratigraphy of paralic coal-bearing strata: an overview. Int. J. Coal Geol. 48 (3–4), 147–179.
Iaccarino, S., Premoli Silva, I., Biolzi, M., Foresi, L.M., Lirer, F., Turco, E., Petrizzo, M.R., 2007. Practical Manual of Neogene Planktonic Foraminifera, p. 141.
IUSS Working Group WRB, 2015. World reference base for soil resources 2014, update 2015 International soil classification system for naming soils and creating legends for soil maps. In: World Soil Resources Reports No. 106. FAO, Rome, p. 192.
Jerrett, R.M., Hodgson, D.M., Flint, S.S., Davies, R.C., 2011. Control of relative sea level and climate on coal character in the Westphalian C (Atokan) Four Corners Formation, Central Appalachian Basin, USA. J. Sediment. Res. 81 (6), 420–445.
Kaïho, K., 1994. Benthic foraminiferal dissolved-oxygen index and dissolved-oxygen levels in the modern ocean. Geology 22, 719–722.
Kennett, J.P., Srinivasan, S., 1983. Neogene Planktonic Foraminifera: A Phylogenetic Atlas. Hutchinson Ross Publishing Company, Stroudsburg, Pennsylvania, p. 265.
Kidwell, S.M., Holland, S.M., 1991. Field description of coarse bioclastic fabrics. Palaios 426–434.
Kirschvink, J.L., 1980. The least-squares line and plane and the analysis of palaeomagnetic data. Geophys. J. Int. 62 (3), 699–718.
Koho, K.A., Piña-Ochoa, E., 2011. Benthic foraminifera: Inhabitants of low-oxygen environments. In: Anoxia: Evidence for Eukaryote Survival and Paleontological Strategies. Springer Netherlands, Dordrecht, pp. 249–285.
Kucera, M., 2007. Planktonic Foraminifera as Tracers of Past Oceanic Environments. In: Hillaire-Marcel, C., de Vernal, A. (Eds.), Methods in Late Cenozoic Paleoceanography. Elsevier Eds., pp. 225–266
Lazzarotto, A., Sandrelli, F., Foresi, L.M., Mazzei, R., Salvatorini, G., Cornamusini, G., Pascucci, V., 2002. Note Illustrative della Carta Geologica d'Italia alla scala 1:50.000 "Foglio 295 - Pomarance". Servizio Geologico d'Italia, Roma, p. 140.
Lirer, F., Foresi, L.M., Iaccarino, S.M., Salvatorini, G., Turco, E., Cosentino, C., Sierro, F. J., Caruso, A., 2019. Mediterranean neogene planktonic foraminifer biozonation and biochronology. Earth Sci. Rev. 196, 102869.
Lisiecki, L.E., Raymo, M.E., 2005. A Pliocene-Pleistocene stack of 57 globally distributed benthonic δ18O records. Paleoceanography 20 (1).
Loeblich, A.R., Tappan, H., 1988. Foraminiferal Genera and Their Classification, 1.2. Van Nostrand Reinhold Company, New York, p. 970.
Lowrie, W., 1990. Identification of ferromagnetic minerals in a rock by coercivity and unblocking temperature properties. Geophys. Res. Lett. 17 (2), 159–162.
Mack, G.H., Tabor, N.J., Zollinger, H.J., 2010. Palaeosols and sequence stratigraphy of the lower Permian Abo Member, South-Central New Mexico, USA. Sedimentology 57, 1566–1583.
Martini, I., Aldinucci, M., 2017. Sedimentation and basin-fill history of the pliocene succession exposed in the northern Siena-Radicofani basin (Tuscany, Italy): a sequence-stratigraphic approach. Riv. Ital. Paleontol. Stratigr. 123 (3), 407–432.
Martini, I., Sandrelli, F., 2015. Facies analysis of a pliocene river-dominated deltaic succession (Siena basin, Italy): implications for the formation and infilling of terminal distributary channels. Sedimentology 62 (1), 234–265.
Martini, I., Foresi, L.M., Bambini, A.M., Riforgiato, F., Ambrosetti, E., Sandrelli, F., 2016. Calcareous plankton bio-chronostratigraphy and sedimentology of the "I Sodi" section (Siena basin, Italy): a key section for the uppermost neogene marine deposition in the inner northern Apennines. Ital. J. Geosci. 135 (3), 540–547.
Martini, I., Ambrosetti, E., Brogi, A., Aldinucci, M., Zwaan, F., Sandrelli, F., 2021. Polyphase extensional basins: interplay between tectonics and sedimentation in the Neogene Siena-Radicofani Basin (Northern Apennines, Italy). Int. J. Earth Sci. 110 (5), 1729–1751.
Medici, M.C., Ceci, M.E., Gliozzi, E., 2011. Early pliocene brackish and freshwater ostracoda from the Valdelsa Basin (Tuscany, Central Italy). Riv. Ital. Paleontol. Stratigr. 117, 473–500.
Meisch, C., 2000. Freshwater Ostracoda of Western and Central Europe, 75(9). Spektrum Akademischer Verlag, Heidelberg, pp. 1158–1159.
Merla, G., Bortolotti, V., 1967. Note Illustrative Della C.G.I. in Scala 1:100.000. Foglio 113 Castelfiorentino (II Edizione). Serv. Geol. It., p. 62
Merla, G., Bortolotti, V., Passerini, P., 1967. Note illustrative della C.G.I. in scala 1: 100.000. Foglio 106 Firenze (II Edizione). Serv. Geol. It., p. 61
Milaneschi, L., Cornamusini, G., Martini, I., Conti, P., Liberato, G.P., Tavarnelli, E., Foresi, L.M., 2024. Shallow-water clastic carbonates of the Southwestern margin of Valdelsa Neogene Basin. Preliminary data on Mid-Pliocene Warm Period in Southern Tuscany (Italy). Rend. Online Soc. Geol. It. 2023, 53–59.
Miller, K.G., Wright, J.D., Browning, J.V., Kulpecz, A., Kominz, M., Naish, T.R., Cramer, B.S., Rosenthal, Y., Peltier, R., Sosdian, S., 2012. High tide of the warm pliocene: implications of global sea level for antarctic deglaciation. Geology 40 (5), 407–410.
Mirabella, F., Braun, T., Brogi, A., Capezzuoli, E., 2022. Pliocene–Quaternary seismogenic faults in the inner Northern Apennines (Valdelsa Basin, southern Tuscany) and their role in controlling the local seismicity. Geol. Mag. 159 (6), 853–872.
Mudelsee, M., Raymo, M.E., 2005. Slow dynamics of the northern hemisphere glaciation. Paleoceanography 20 (4).
Murray, J.W., 1968. Living foraminifers of lagoons and estuaries. Micropaleontology 435–455.
Murray, J.W., 1991. Ecology and Paleoecology of Benthonic Foraminifera. Longman Scientific and Technical, Essex, England, p. 397.
Murray, J.W., 2006. Ecology and Applications of Benthonic Foraminifera. Cambridge University Press, p. 426.
Nalin, R., Ghinassi, M., Foresi, L.M., Dallanave, E., 2016. Carbonate deposition in restricted basins: a pliocene case study from the Central Mediterranean (Northwestern Apennines), Italy. J. Sediment. Res. 86 (3), 236–267.
Odin, G.S., Matter, A., 1981. De glauconiarum origine. Sedimentology 28 (5), 611–641.
Ogg, J.G., 2020. Geomagnetic polarity time scale. In: Geologic Time Scale 2020. Elsevier, pp. 159–192.
Pascucci, V., Merlini, S., Martini, I.P., 1999. Seismic stratigraphy of the Miocene-Pleistocene sedimentary basins of the Northern Tyrrhenian Sea and Western Tuscany (Italy). Basin Res. 11, 337–356.
Peharda, M., Walliser, E.O., Markulin, K., Purroy, A., Uvanović, H., Janeković, I., Župan, I., Vilibić, I., Schöne, B.R., 2019. Glycymeris pilosa (bivalvia) - a high-potential geochemical archive of the environmental variability in the Adriatic Sea. Mar. Environ. Res. 150, 104759.
Poag, C.W., 1981. Ecologic Atlas of Benthonic Foraminifera of the Gulf of Mexico. Marine Science International, Woods Hole, Massachusetts, p. 174.
Poneti, G., Benvenuti, M., Scarselli, N., Craig, J., Sani, F., 2024. Integrated analysis of the Neogene–Quaternary Valdera-Volterra Basin (Northern Apennines). Evidence for composite development of hinterland basins. Basin Res. 36 (5), 12897.
Retallack, G.J., 2001. Soils of the Past: An Introduction to Paleopedology. John Wiley & Sons.
Riforgiato, F., Foresi, L.M., Mazzei, R., Salvatorini, G., Sandrelli, F., 2005. Chronostratigraphic revision of some Pliocene basins in Tuscany at the Zanclean/ Piacenzian boundary. Boll. Soc. Geol. Ital. 7–13.
Riforgiato, F., Foresi, L.M., Di Stefano, A., Aldinucci, M., Pelosi, N., Mazzei, R., Salvatorini, G., Sandrelli, F., 2011. The Miocene/Pliocene boundary in the mediterranean area: new insights from a high-resolution micropalaeontological and cyclostratigraphical study (cava serredi section, Central Italy). Palaeogeogr. Palaeoclimatol. Palaeoecol. 305 (1–4), 310–328.
Rohling, E.J., 1994. Review and new aspects concerning the formation of Eastern Mediterranean Sapropels. Mar. Geol. 122, 1–28.
Rossignol-Strick, M., 1983. African monsoons, an immediate climate response to orbital insolation. Nature 304, 46–49.
Sani, F., Bonini, M., Piccardi, L., Vannucci, G., Delle, Donne D., Benvenuti, M., Moratti, G., Corti, G., Montanari, D., Sedda, L., Tanini, C., 2009. Late Pliocene-Quaternary evolution of outermost hinterland basins of the Northern Apennines (Italy), and their relevance to active tectonics. Tectonophysics 476, 336–356.
Tolderlund, D.S., Bé, A.W.H., 1971. Seasonal distribution of planktonic foraminifera in the Western North Atlantic. Micropaleontology 17, 297–329.
Van Voorthuysen, J.H., 1973. Foraminiferal ecology in the Ria de Arosa, Galicia, Spain. Zool. Verh. 123 (1), 1–68.
Walton, W.R., Sloan, B.J., 1990. The genus ammonia bruennich, 1772; its geographic distribution and morphologic variability. J. Foram. Res. 20 (2), 128–156.
Wright, V.P., Marriott, S.B., 1993. The sequence stratigraphy of fluvial depositional systems: the role of floodplain sediment storage. Sediment. Geol. 86 (3–4), 203–210.
www.foraminifera.eu.
www.marinespecies.org.